Fisheries and Oceans Canada | Pêches et Océans Canada
Ecosystems and Oceans Science | Sciences des écosystèmes et des océans

**Canadian Science Advisory Secretariat (CSAS)**

**Research Document 2020/033**

**Quebec region**

# Significance of dominant zooplankton species to the North Atlantic Right Whale potential foraging habitats in the Gulf of St. Lawrence: a bio-energetic approach

Caroline Lehoux, Stéphane Plourde, Véronique Lesage

Fisheries and Oceans Canada
Institut Maurice-Lamontagne
850, Route de la Mer
Mont-Joli, Québec Canada G5H 3Z4

September 2020

Canada

**Foreword**

This series documents the scientific basis for the evaluation of aquatic resources and ecosystems in Canada. As such, it addresses the issues of the day in the time frames required and the documents it contains are not intended as definitive statements on the subjects addressed but rather as progress reports on ongoing investigations.

**Published by:**

Fisheries and Oceans Canada
Canadian Science Advisory Secretariat
200 Kent Street
Ottawa ON K1A 0E6

http://www.dfo-mpo.gc.ca/csas-sccs/
csas-sccs@dfo-mpo.gc.ca


ISSN 1919-5044

**Correct citation for this publication:**

Lehoux, C., Plourde S., and Lesage, V. 2020. Significance of dominant zooplankton species to the North Atlantic Right Whale potential foraging habitats in the Gulf of St. Lawrence: a bio-energetic approach. DFO Can. Sci. Advis. Sec. Res. Doc. 2020/033. iv + 44 p.

***Aussi disponible en français :***

*Lehoux, C., Plourde S., et Lesage, V. 2020. Importance des espèces dominantes de zooplancton pour les habitats potentiels d'alimentation des baleines noires de l'Atlantique Nord dans le golfe du Saint Laurent : une approche bioénergétique. Secr. can. de consult. sci. du MPO. Doc. de rech. 2020/033. iv + 45 p.*

## TABLE OF CONTENTS

ABSTRACT ..... iv
INTRODUCTION ..... 1
MATERIAL AND METHODS ..... 2
ZOOPLANKTON DATA ..... 2
VERTICAL DISTRIBUTION AND 3D PREYSCAPE ..... 3
HABITAT SUITABILITY – BIOENERGETICS MODEL ..... 4
RESULTS ..... 5
ZOOPLANKTON VERTICAL DISTRIBUTION ..... 5
BIO-ENERGETIC MODEL SENSITIVITY ..... 6
PREYSCAPE ..... 6
HABITAT SUITABILITY ..... 7
TEMPORAL VARIATION IN HABITAT SUITABILITY ..... 7
DISCUSSION ..... 8
SOURCES OF UNCERTAINTIES ..... 9
REFERENCES CITED ..... 11
TABLES ..... 16
FIGURES ..... 20
APPENDIX 1 ..... 36
APPENDIX 2 ..... 40
APPENDIX 3 ..... 44

## ABSTRACT

The North Atlantic Right Whale (NARW) is an endangered species that feeds primarily on *Calanus finmarchicus* in their traditional feeding areas in the western North Atlantic. In recent years, the Gulf of St. Lawrence (GSL) was identified as an important feeding ground for this population. In this region, the large and lipid-rich *C. finmarchicus*, *C. hyperboreus* and *C. glacialis* are abundant species, but other small calanoids such as *Pseudocalanus* spp. and *Temora* spp. and krill are also numerically abundant. Since the diet of NARW is unknown in the GSL, the potential relative contribution of these prey to NARW in early and late summer between 2006 and 2017 was assessed using a bioenergetics model. The model used a 3D preyscape, which was predicted using the depth-integrated biomass of zooplankton and species-specific vertical distributions. The model assessed the energy gained according to prey density in each 10 m-depth bins, and the energy requirement of mature females that were resting, pregnant or lactating. A suitable habitat was defined as a positive difference between the energy gained and the energy required divided by the energy required. The difference in habitat suitability between the period before and after 2010 was assessed as well as the sensitivity to model parameters. The effect of zooplankton vertical distribution on their availability to NARW, and the relationship between habitat suitability and bathymetry were also examined. *C. hyperboreus* was identified as the prey contributing the most energy to NARW compared to the other prey species. This was true with the exception of the southwestern GSL in August-September when *C. finmarchicus* contribution increased relative to the June-July period. The contribution of other prey species was overall negligible. The southwestern GSL was identified as the most suitable habitat for NARW in June-July, whereas the northern GSL, and more specifically the area to the north of Anticosti Island was identified as the most suitable habitat in August-September. Using the model parameters minimizing net energy gain, there were almost no habitats that provided sufficient energy for NARW to meet their daily energy requirements. When using the model parameters maximizing the net energy gain, very large areas that encompassed more than 50% of the southwestern GSL in June-July and the northern GSL in August-September appeared suitable. While the energy gained did not markedly decrease in the northern GSL between 2006-2010 and 2011-1017, it did decrease in the southwestern GSL, resulting in a lesser persistence of NARW suitable habitat in the region during the latter period. The distribution of NARW suitable habitats changed between the two periods, with suitable areas in the Shediac Valley and on the Orphan Bank in June-July, and to the north of Anticosti Island in August-September being larger in 2011-2017 compared to the 2006-2010 period. In recent years, the abundance of large *Calanus* species decreased while the abundance of small calanoids tended to increase. If this trend continues, the energy available to NARW is likely to decrease and possibly not be sufficient to meet their energy requirements.

## INTRODUCTION

The North Atlantic right whale (*Eubalaena glacialis*; NARW from here on) belongs to the mysticetes, a family that shares the characteristic of having baleen plates. NARW employ a ram filtration feeding technique, which involves passively filtering large volumes of zooplankton-filled water through these baleen plates, by slowly swimming forward with mouth agape (Mayo and Marx 1990). While different prey can be encountered when using filter feeding, their capturability depends on prey avoidance capacity and filterability (Mayo et al. 2001). By studying the morphology of baleen plates from a juvenile NARW, Mayo et al. (2001) determined that filtering efficiency decreases with decreasing prey size. NARW appear well adapted for harvesting larger lipid-rich mesozooplankton such as the later life stages of species such as *Calanus finmarchicus*, but less so for smaller organisms unless they are found in exceptional densities (Mayo et al. 2001). For macrozooplankton, filterability may be high but capture efficiency may be reduced by a greater avoidance capacity in these species compared to the slow ramming speed of a feeding right whale, which is estimated at approximately 1 m $s^{-1}$ (Nousek McGregor 2010; Baumgartner and Mate 2003; van der Hoop et al. 2019). Feeding on these highly mobile species would require ramming at a much higher speed, increasing the energetic costs of feeding, a behaviour that has been documented in Southern right whales (Hamner et al. 1988).

Multiple studies have demonstrated that NARW feed primarily on later life stages (C4 or older) of *Calanus finmarchicus* when in their traditional feeding grounds in the western North Atlantic, i.e., Cape Cod Bay, Great South Channel, lower Bay of Fundy, Roseway Basin and Jeffreys Ledge (reviewed in Baumgartner et al. 2007). However, NARW can also consume other meso and macrozooplankton species, including *Pseudocalanus* spp., *Centropages* spp., and occasionally larval barnacles and euphausiids (or krill) (Watkins and Schevill 1976; Murison and Gaskin 1989; Mayo and Marx 1990; Collet 1909). Other calanoid copepod species, such as *C. glacialis* and *C. hyperboreus* have been collected on NARW feeding grounds and potentially within NARW fecal matter and thus, represent potential prey of NARW (Kraus and Prescott 1982; Murison and Gaskin 1989; Murison 1986). These inferences about NARW diet are based largely on direct observation of surface skim-feeding, on the occurrence of NARW in areas with high densities of these copepods (Kenney et al. 1986, 1995, Michaud and Taggart 2007, Wishner et al. 1988) or, for NARW not feeding at the surface, on net sampling zooplankton community in their vicinity (reviewed in Baumgartner et al. 2007). In the latter case however, inference of the species targeted by NARW in regions where several species might be abundant, or where a vertical stratification exists in their distribution may not be possible.

A recent increase in dedicated survey effort in the Gulf of St. Lawrence (GSL) indicates that this feeding ground may be more important than previously thought (DFO 2019). In this region where the diet of NARW has not been studied, large-bodied and lipid-rich copepods of the genus *Calanus* dominate the mesozooplankton biomass, with *Calanus hyperboreus*, the largest *Calanus* species, forming the bulk of the biomass (Sorochan et al. 2019). Small calanoid copepods such as *Pseudocalanus spp.* and *Temora spp.* are also numerically abundant in the GSL, representing a relatively high proportion of the mesozooplankton community in this region, particularly in the shallow southwest GSL (SWGSL) (Devine et al. 2017). At the other end of the zooplankton size spectrum, krill represents an important component of the GSL ecosystem, forming dense aggregations across the region, including some areas in the SWGSL (McQuinn et al. 2016, Plourde et al. 2016). Although previous studies indicate that *C. finmarchicus* represents the main prey of NARW, the lack of information about NARW diet in the GSL and the predominance of a large, energetically-rich prey with low motility such as *C. hyperboreus*, raise questions about its potential importance for NARW in this region.

The main objective of this study was to quantify the potential contribution of different abundant zooplankton taxa to NARW foraging in the GSL. More specifically, we used an approach previously developed (Gavrilchuk et al. 2020) using a bio-energetic model of NARW foraging combined with 3-D preyscape to assess the potential net energy gain as a measure of habitat suitability for NARW foraging on the following zooplankton taxa: *C. finmarchicus/C. glacialis*, *C. hyperboreus*, *Pseudocalanus spp.*, *Temora spp*. and krill (*Meganyctiphanes norvegica*, *Thysanoessa* spp). We also aimed to address four secondary objectives: (1) quantifying the impact of zooplankton diel vertical migrations on their availability to NARW, (2) assessing the distribution of suitable foraging habitats in relation to bathymetry, (3) evaluating model sensitivity to parameter uncertainty, and (4) comparing the suitable habitat distribution before (2006-2010) and after (2011-2017) the change in NARW population summering distribution, which approximately coincided with a change in *Calanus* biomass patterns (Pettis et al. 2018, Sorochan et al. 2019).

# MATERIAL AND METHODS

## ZOOPLANKTON DATA

We used spatially-explicit mesozooplankton data collected in the GSL between 2006 and 2017 (Figure 1, A.1.1), the same period considered for *Calanus* species by Gavrilchuk et al. (2020). We separated the data into two seasons that roughly matched the timing of the sampling surveys. The June-July data were mainly collected in June as part of the Mackerel egg survey in the SWGSL and the Atlantic Zone Monitoring Program (AZMP) that samples different oceanographic lines across the SWGSL and the northwest (NWGSL) and northeast (NEGSL) GSL (Figure 1). The August-September data were collected during the Multidisciplinary surveys in the NWGSL-NEGSL (August) and the SWGSL (September) (Figure 1B). Additionally, we included the data collected at a high-frequency AZMP sampling site located in the SWGSL, i.e., the Shediac Valley station (Figure 1). Zooplankton samples were collected either with double oblique 333-µm Bongo tows (Mackerel egg survey) or with standard AZMP vertical tows (200-µm mesh net) (Devine et al. 2017). Details related to sample analysis and zooplankton data standardization among sampling programs are presented elsewhere (Plourde et al. 2019; Sorochan et al. 2019).

We used two different sources of data to describe the spatial distribution of krill, and assess the its importance to NARW. First, we used krill biomass estimated from multi-frequency acoustic surveys (38, 70, 120, 200, 333 kHz) conducted in the northern GSL (NGSL) in June (DFO AZMP survey) and August (DFO multidisciplinary survey) from 2008 to 2015 to describe krill spatial distribution (Figure 1C-D, Figure A1.2). Acoustic data were integrated in 0.5 km bins in which the biomass of three groups was estimated: *Meganyctiphanes norvegica*, *Thysanoessa* ssp. and a “mixed’’ category. Technical details on the sampling and processing of acoustic data are available in McQuinn et al. (2013, 2015). Secondly, we used krill abundance data obtained from the analysis of BONGO samples collected during the Mackerel egg survey in June from 1998 to 2003 in the SWGSL (Figure 1C). Krill data were corrected for net avoidance during day and night (Weibe et al. 2004, 2013, Simard and Sourisseau 2009, J.-F. St-Pierre et al. DFO Quebec Region, unpublished data) and for sampled depth using krill vertical distribution (see below) (Plourde et al. 2019, Gavrilchuk et al. 2020). Although not collected during the 2006-2017 period, these net sampled krill data were deemed more reliable than the krill and/or plankton categories obtained by acoustic sampling in the SWGSL. In this shallow area, *Calanus* and krill vertical distributions can overlap in dense scattering layers near the bottom during daytime, resulting in a greater potential for these taxa to be confounded and misclassified than in the deeper NGSL (McQuinn et al. 2015).

Abundance of copepod species was transformed to dry weight biomass (Dw) using stage and species-specific individual dry weight (mg $m^{-2}$). Biomass was transformed to depth-integrated energy (kJ $g^{-1}$ $m^{-2}$) using species-specific energy density from the literature (kJ $g^{-1}$, Table 1) (Brey et al. 2010, Davies et al. 2012). Data analyses were restricted to the late stages CIV-CVI of *Calanus spp*. and to the CV-CVI stages of *Pseudocalanus spp*. and *Temora spp.* because they are captured with the most efficiency by NARW (Mayo et al. 2001). Because *Pseudocalanus* spp and *Temora* spp data at the Shediac Valley station are not stage-specific, total abundance collected with the 200-µm AZMP net was used.

## VERTICAL DISTRIBUTION AND 3D PREYSCAPE

We applied the approach used by Plourde et al. (2019) and Gavrilchuk et al. (2020) to build 3-D preyscapes for the different zooplankton taxa. These 3-D preyscapes are essential to the assessment of NARW potential foraging success in the region.

The vertical distribution of biomass (cumulative percentage of biomass with depth, $pDW_{cum}$) was described for each copepod species using Generalized Additive Models (GAMs) to (1) correct the biomass at stations where less than 95% of the water column was sampled and (2) to parameterize the 3D preyscape. The GAMs were similar to Plourde et al. (2019) with some modifications necessary to meet our objectives. In the present study, GAMs were fitted separately for night and day in June-July and August-September. The data used to fit the GAMs represented a subset of the data used by Krumhansl et al. (2018) and Plourde et al. (2019) (Figure A.1.3). No seasonal difference in the vertical distribution of *Pseudocalanus spp*. and *Temora spp*. were detected, and only two models, one daytime and one nighttime, were fitted for each species. Since the vertical distribution of these smaller copepod species does not change with seasons, all available data up to November were used to improve sample size for these species. GAMs followed a beta distribution and the predictor variables included station depth (Z) and percentage of depth sampled (%Z) and their interaction in order to consider the effect of variations in bathymetry on vertical distribution (Krumhansl et al. 2018, Plourde et al. 2019).

There was no benefit to using similar GAMs to model krill vertical distribution because all sampled stations were located in deeper areas of the GSL. The vertical distribution of $pDW_{cum}$ was therefore described using either a sigmoidal (daytime) or a hyperbola (nighttime) function fitted to data collected with a 1-$m^2$ BIONESS equipped with a strobe light (Table 3). Distinct models were fitted for the NWGSL and NEGSL during daytime because krill daytime vertical distribution in the NWGSL is affected by dissolved organic matter associated with freshwater which affects the surface layer and light penetration (Plourde et al. 2014, McQuinn et al. 2015). The vertical distributions of krill in the SWGSL and NWGSL were assumed to be similar due to the strong freshwater influence in these regions (Galbraith et al. 2018).

Spatial climatologies of zooplankton depth-integrated energy were created for each zooplankton taxa for the 2006-2017 period. One data grid (10 x 10 $km^2$) was created for each species and season (June-July, August-September). All maps used a grid with a resolution of 10 km², and were created using the “raster” package (v.2.7-15; Hijmans 2018). The geographic coordinate system references were from the North American Datum (Nad83) with a Lambert conformal conic reference projection (Québec, Canada). The mean of each variable was averaged in each 10 x 10 km grid cell and interpolated to a maximum distance of 30 km using ordinary kriging or using inverse distance weighted interpolation when no spatial structure was detected. Geostatistical models were performed with the “gstat” package (v. 1.1-6, Pabesma 2004, Gräler et al. 2016).

The vertical distribution models were used to build daytime and nighttime 3D preyscape for each zooplankton taxon using each station sampled between 2006 and 2017. The depth-integrated biomass (kJ $m^{-2}$) was multiplied by the proportion of the energy in each 10-m thick vertical layer predicted by the vertical distribution models to obtain a vertical profile of the energy density (kJ $m^{-3}$) necessary for the bio-energetic foraging model (see below).

## HABITAT SUITABILITY – BIOENERGETICS MODEL

A bio-energetic foraging model accounting for the annual energetic costs of NARW was combined with the species- and season-specific 3D preyscapes to predict areas where the energy gains would exceed energy requirements of NARW, i.e. locations that would be suitable for foraging NARW (see Gavrilchuk et al. 2020). The bio-energetic foraging model was applied to all discrete zooplankton data considered in our study (stations sampled with plankton nets, and 0.5 km horizontal bins for acoustic data)

Including zooplankton taxa spanning a wide range of body size (1 to 40 mm) in the preyscape implies considering taxa-specific NARW foraging efficiency, i.e. the filtering efficiency of baleens when feeding on smaller organisms, and NARW capture efficiency when pursuing larger and more motile prey. NARW baleen shows a filtering efficiency comparable to a 333-µm mesh net (Mayo et al. 2001), which results in a filtering efficiency approaching 1.0 for late stages of *Calanus* species (> 1.5 mm body length), and of 0.5 for late stages *Pseudocalanus* and *Temora* (< 1 mm body length) (Nichols and Thompson 1991). Therefore, NARW baleen would capture 50% of the *Pseudocalanus/Temora* late stages sampled with the 200-µm AZMP net while no correction for efficiency would be needed for data issued from 333-µm bongo net sampling (Table 1). At the other end of the size spectrum, adult krill has high swimming capabilities, and a highly cohesive behavior while aggregated, resulting in a capacity to avoid large plankton nets not equipped with a strobe light (Sameoto et al.1993, Wiebe et al. 2004, Simard and Sourisseau 2009). We therefore implicitly considered that the capture efficiency of NARW with a mouth area of 1.7-1.9 $m^2$ (van der Hoop et al. 2019) and an averaged swimming speed during their feeding in zooplankton layers of 1.0 m $s^{-1}$ (Nousek McGregor 2010; Baumgartner and Mate 2003) would be equivalent to a 1-$m^2$ plankton net equipped with 333-µm mesh nets towed at 1.1-1.3 m $s^{-1}$ (or 2.5-3.0 knots). The efficiency of a 1-$m^2$ BIONESS with and without a strobe light to capture *M. norvegica* and *T. raschii* during day or night was assessed during two distinct field experiments in the GSL (J.-F. St-Pierre and I. McQuinn, DFO Quebec Region, pers. comm.). The capture efficiency of nets without the strobe was significantly lower relative to the sampling with a strobe (0.035-0.27), and was lower for both species when sampling during the day than at night (Table 1). Capture efficiency of nets without the strobe was also lower for *T. raschii* than *M. norvegica,* particularly during daytime (0.035 vs 0.17) (Table 1). These species-specific results correspond to previous studies targeting the whole krill assemblage (Weibe et al 2004, 2013, Simard and Sourisseau 2009).

Species-specific capture efficiency coefficients ($\varepsilon_c$) (Table 1), i.e. the proportion of each species *in situ* available energy captured by NARW, were then considered as a new parameter to calculate the energy gain ($E_{in}$):

$$E_{in} = A_m U_b T_b E_p D_p \varepsilon_A \varepsilon_c$$

Where $A_m$ is the mouth opening area (1.7-1.9 m²), $U_b$ is the swim speed during feeding (1 m $s^{-1}$), Tb is the time spent ingesting prey (sec day $^{-1}$), $E_p$ and $D_p$ are the prey energetic content (MJ $g^{-1}$, table 1) and density (g $m^{-3}$), respectively, and $\varepsilon_A$ is the assimilation efficiency (0.80-0.92). For details, see Gavrilchuk et al. (2020).

We estimated the $E_{in}$ and the energy cost ($E_{out}$) associated with foraging on each prey species separately and for different combination of species: *Calanus spp.* (*C. finmarchicus*, *C.*

*hyperboreus*), copepods (*Calanus spp*., *Pseudocalanus spp.* and *Temora spp*), and total biomass (copepods and krill). For each station, we calculated $E_{in}$ and $E_{out}$ assuming that the NARW dive to where the 10 m-bin $E_{net}$ is maximum (Baumgartner et al. 2003, Baumgartner et al. 2017).

A separate preyscape was produced for day and night, allowing the bioenergetics model to estimate energy gain ($E_{in}$) and energy requirement ($E_{out}$) for different depth layer during the two periods. A single value representative of 24 h was obtained by weighing the mean of the day and night $E_{in}$ and $E_{out}$ by day and night duration according to seasons. In June-July, daytime was estimated at 16 h, and nighttime at 8 h, whereas in August-September, their respective duration was 13.4 and 10.6 hs. Daytime duration was calculated using the maptools package in R (v. 0.9-4, Bivand and Lewin-Koh 2018). The net energy index ($E_{net}$) was calculated from these corrected $E_{in}$ and $E_{out}$ as:

$$E_{net} = \frac{E_{in} - E_{out}}{E_{out}}$$

Sensitivity of habitat suitability to model parameters was assessed using the models for resting, pregnant and lactating females. Parameters that contributed to the minimum $E_{in}$ and maximum $E_{out}$ were combined to provide minimum $E_{net}$, whereas parameters that contributed to maximum $E_{in}$ and minimum $E_{out}$ were combined to provide maximum $E_{net}$. The parameters allowed to vary in the $E_{in}$ equation were the mouth area (1.7-1.9 m², van der Hoop et al. 2019), time spent foraging per day (15.1-17.2 h), prey energy density (Table 1), and assimilation efficiency (0.80-0.92). The $E_{out}$ varied according to the uncertainty in travel time during summer (6.2-8.3 h) and winter (19.9-21.4 h), calf mass (pregnant females only; 1101 ± 311 kg) and calf energy requirement (lactating females only; 1767 ± 261 MJ/d), residency time on wintering grounds (resting and pregnant females: 26.1-55.5 d; lactating females: 78.9-99.6 d) (Kryzstan et al. 2018).

We assessed the difference in energy gain ($E_{in}$) and depth-integrated energy among taxa with two Kruskall-Wallis tests using the 'PMCMRplus' package (v.1.4.1, Thorsten 2018) in R. We examined pairwise differences among taxa with the Dunn's non-parametric all-pairs comparison test (Dunn 1964), and evaluated the difference in $E_{in}$ between the two periods (2006-2010 and 2011-2017) using the same approach. The large number of very small values prevented the use of parametric methods such as the analysis or variance (ANOVA) or Generalized Linear Models.

To detect suitable areas ($E_{net}$ >0) and represent the inter-annual variability in habitat suitability, we created an interpolated layer of $E_{net}$ for each year, season and taxa using the kriging approach described above. In each cell, we calculated the percentage of years for the periods 2006-2017, 2006-2010 and 2011-2017 where $E_{net} > 0$. We also applied the model to the data at the station level to represent the temporal variation in $E_{net}$ at the Shediac station, and to describe the relationship between $E_{net}$ and bathymetry for the period 2006 to 2017.

# RESULTS

## ZOOPLANKTON VERTICAL DISTRIBUTION

GAMs accurately modelled the vertical distribution of the cumulative percentage of dry weight ($pDW_{cum}$) of the different prey taxa (Table 2). The Spearman's correlation coefficient between the predicted and observed $pDW_{cum}$ varied between 0.78 and 0.93. Models for the daytime vertical distribution performed slightly better than the nighttime models. We selected station depth (Z) and percentage of station sampled (%Z) as the interaction term for GAMs fitted to

daytime vertical distributions of *C. finmarchicus* and *C. hyperboreus* in June, and daytime vertical distribution of *Temora spp*. Given that *C. hyperboreus* enters diapause around June, a single model not accounting for diel vertical migrations (DVM) was used for August-September. GAMs partial effects plots are presented in Appendix 2.

DVM were observed in the different copepod taxa, and were represented for a station 100 m deep (Figure 2-3). A fraction of *C. finmarchicus* performed DVM in June-July and August-September leading to two biomass maxima occurring at 10-20 m and 50-75 m at night, and only one peak occurring at 50-75 m during daytime (Figure 2). Only a small proportion of *C. hyperboreus* was observed in the upper layer (10-30 m) at night in June-July, as nearly 100% of the biomass remained in the deeper layers at 75 m in August-September (Figure 2). *Pseudocalanus spp.* showed two density maxima, above and below 50 m respectively, during day and night with the peak in the upper layer being greater and shallower at night than during the day (Figure 3). The vertical distribution of *Temora spp.* was highly sensitive to station depth. Its distribution during the night was generally more homogeneous across the water column compared to daytime (Figure 3).

Krill vertical distribution was well predicted by the models with either a hyperbola (night) or a sigmoidal (day) function with $R^2$ between 0.66 and 0.94 (Table 3). The nighttime distribution was predicted with less accuracy than daytime distribution for both *M. norvegica* and *T. raschii*. The daytime vertical distribution of *M. norvegica* was concentrated at deeper depths compared to *T. raschii*. *T. raschii* was found at deeper depth during daytime in the NEGSL than the NWGSL (Figure 4), whereas during nighttime, the two species distributed very similarly with the peak biomass located near the surface (Figure 4).

## BIO-ENERGETIC MODEL SENSITIVITY

Predictions from the bio-energetic model about the location (% of 10 km x 10 km cells) and temporal persistence (% of years) of grid cells where $E_{net}$ exceeded 0 were sensitive to NARW reproductive state (resting, pregnant, lactating) and to variations in other model parameters (Table 4). Overall, the increase in energy requirements for females going from a resting to a pregnant and lactating state, and the set of model parameter values minimizing $E_{net}$ reduced the size and temporal persistence of suitable areas (Table 4). Since the impact of NARW reproductive state on the identification of suitable habitats is explicitly addressed in another study (Gavrilchuk et al. 2020), we performed our analyses using an intermediate scenario, i.e., we used pregnant females and a set of model parameters resulting in an averaged $E_{net}$.

The sensitivity of the foraging bio-energetic model to copepod DVM was low, given that depths where $E_{net} \geq 0$ did not vary between day and night, among seasons or regions, and that positive $E_{net}$ were met at 75% to 100% of station depths (Figure 5). The model was more sensitive to krill DVM, i.e., NARW would gain more energy on the surface layer at night and the deep layer during daytime, but with no incidence on our results since all $E_{net}$ were < 0 (Figure 6).

## PREYSCAPE

The depth-integrated energy acquired by feeding on different taxa varied significantly among all pairs of taxa tested ($p < 0.0001$) except for *Pseudocalanus* spp. versus *Temora* spp, which provided similar amounts of energy ($p = 0.06$). The depth-integrated energy was dominated by *Calanus* species both in the NGSL and SWGSL during the 2006-2017 period (Figure 7). In the NGSL, *C. hyperboreus* depth-integrated energy was 6-10 times greater than for *C. finmarchicus* in June-July and August-September, with krill depth-integrated energy ranking third in both seasons (Figure 7A-B). *Pseudocalanus* spp. and *Temora* spp. contributions were 1-2 orders of magnitude lower than *Calanus* (Figure 7A-B). In the shallower SWGSL, *C. hyperboreus*

contributed 2-4 times more energy than *C. finmarchicus* in June-July, but the situation reversed in August-September with *C. finmarchicus* representing 8-9 times more energy than *C. hyperboreus* (Figure 7C-D). This seasonal change in the contribution of both species was associated to an increase in the depth-integrated energy of *C. finmarchicus*, and to a decrease in that of *C. hyperboreus* between June-July and August-September (Figure 7C-D). In the SWGSL, krill did not contribute more than the smaller copepod species as opposed to findings for the NGSL. *Pseudocalanus* depth-integrated energy also increased from June-July to August-September in the SWGSL (Figure 7). The spatial distribution and inter-annual variation of the depth-integrated energy are shown in Figure 8-9 and Appendix 3, respectively.

The energy gain ($E_{in}$) estimated with the bio-energetic foraging model followed a pattern generally similar to the depth-integrated energy, but with species-specific differences associated with variable foraging efficiency of NARW when feeding on different prey (Figure 7). *C. hyperboreus* provided more energy to NARW than the other species in all locations and seasons, except in the SWGSL in August-September when *C. finmarchicus* contribution increased relative to the June-July period. The contribution of other prey species was negligible (Figure 7). The energy gain differed among taxa ($p < 0.0001$; $p=0.02$ for the *Temora* versus *Pseudocalanus* pairwise comparison).

## HABITAT SUITABILITY

Our analyses, based on the percentage of years that a 10 x 10 km grid cell in the 2006-2017 period was estimated to be suitable ($E_{net}>0$), detected large foraging areas in the SWGSL in June-July (Figure 10). These areas were overall not persistent, with cells showing $E_{net}>0$ for a maximum of 40% of the years. These areas extended along a north-to-south axis west and east of the Orphan Bank and covered most of the Shediac Valley, and the area between the Magdalen Islands and Prince Edward Island (PEI) and Cape Breton (Figure 10F, see Appendix 1.4 for the position of topographic and geographic features). The species-specific analyses clearly showed that these areas were mainly associated with *C. hyperboreus* (Figure 10B). No suitable foraging areas were identified in the NGSL in June-July, but the limited spatial coverage in this region probably contributed to this result.

In August-September, two main suitable areas (Figure 11), again mostly associated with *C. hyperboreus*, were identified north of Anticosti Island and in the NEGSL (Figure 11B). Other potential small suitable areas were also highlighted in deeper channels across the NGSL. The SWGSL appeared generally less suitable in August-September than in June-July in accordance with the decrease in depth-integrated energy and energy gained on *C. hyperboreus* (Figure 5), although the spatial coverage of zooplankton sampling in the region was more restricted than in June–July (Fig. 1).

The distribution of suitable habitats (stations with $E_{net} > 0$) in relation to bathymetry markedly differed in the SWGSL and NGSL (Figure 12). In the SWGSL most suitable habitats were associated with bathymetry between 50 m and 150 m with 0.5% of the suitable habitats being observed in regions shallower than 50 m (Figure 12). In the NGSL, 0.04% of the suitable habitats (1 station) were associated with a bathymetry < 100 m, while most of them were observed between 150 m and 350 m (Figure 12).

## TEMPORAL VARIATION IN HABITAT SUITABILITY

The mean potential energy gained by NARW foraging on *Calanus* species tended to decrease between the 2006-2010 and 2011-2017 periods although no significant difference was detected between the two periods (Figure 15, $p = 0.5$). A decrease was observed for NARW foraging on *C. finmarchicus* in the NGSL and SWGSL in both seasons, but it appeared more prominent for

NARW feeding on *C. hyperboreus* in the SWGSL (Figure 15). The energy gained by NARW foraging on *Pseudocalanus* and *Temora* was higher in 2011-2017 relative to 2006-2010, but to a much smaller extent than the decrease observed for *Calanus* species. The potential energy gained by foraging on krill increased between 2006-2010 and 2011-2017 in June-July (Figure 15A), but decreased in the NGSL in August-September (Figure 15B). Overall, the sharp decrease in the potential energy gained by foraging on *Calanus* species in the SWGSL was not compensated by an increase in potential energy gained from feeding on other taxa.

The distribution and persistency of suitable habitats predicted based on the depth-integrated energy of copepods differed between the 2006-2010 and 2011-2017 periods. In June-July 2006-2010, suitable habitats were mostly located in the southernmost half of the GSL in the Shediac Valley, in the Bradelle Bank area and between the Magdalen Islands and Cape Breton as well as east of the Orphan Bank (Figure 16). In June-July 2011-2017, the suitable habitats were less persistent and observed in the Shediac Valley and east of the Gaspé Peninsula on the American bank and west of the Orphan bank (Figure 16). The contribution of species did not change between the two periods in June-July with *C. hyperboreus* providing most of the energy (Figure 16). In August-September, the suitable habitats were patchy in the NGSL with qualitatively larger patches in 2011-2017 than in 2006-2010. In the SWGSL, in August-September, no suitable cells were detected in both periods (Figure 17). In accordance with the decrease in potential energy gained between 2006-2010 and 2011-2017 (Figure 15), the suitable habitats identified in 2011-2017 were overall less persistent than those depicted in 2006-2010 (Figure 16).

Monthly averaged depth-integrated total copepod energy at the Shediac Valley station was rarely suitable ($E_{net} > 0$) during the period 1999-2017 (Figure 18) except in 2003 during June and July. Using the 1998-2003 krill data collected with plankton nets, we estimated that the energy provided by krill near the Shediac Valley station in June would represent 2 % of the energy provided by *Calanus spp*.

## DISCUSSION

The main objective of this study was to determine the energy that different prey may contribute to NARW foraging in the GSL using the approach developed by Gavrilchuk et al. (2020) where a bio-energetic model is coupled to a taxon-specific 3D preyscape. *C. hyperboreus* may provide 10 times more energy to NARW than *C. finmarchicus* in the SWGSL in June-July, and in the NGSL in June-July and August-September. *C. finmarchicus* contribution increased in August-September in the SWGSL, surpassing that of *C. hyperboreus*. *Pseudocalanus spp.*, *Temora spp.* and krill can provide only a very small fraction of the energy required by NARW.

The energy provided by *C. hyperboreus* decreased in the SWGSL from June-July to August-September. *C. hyperboreus* reproduces in winter in deep regions of the GSL. The entry into diapause occurs in June, and is preceded in the spring by a short active period in the surface layer during which *C. hyperboreus* is available to surface transport (Plourde et al. 2003, Plourde et al. 2019). There is no local production as early stages of *C. hyperboreus* are produced in the deeper NWGSL and NEGSL (Plourde et al. 2003, Devine et al. 2017, Brennan et al. 2019). The SWGSL is therefore seeded with *C. hyperboreus* each spring; interruption of supply from deep regions and natural mortality (predation) would be the most likely factors explaining the decrease of *C. hyperboreus* abundance during Summer and Fall in the SWGSL. On the other hand, the energy potentially contributed by *C. finmarchicus* increased in the SWGSL between June-July and August-September. This species remains active until August and can produce a second smaller generation in late Summer-early Fall in the deep regions of the GSL, which makes it available for transport in the SWGSL over a longer time window than *C. hyperboreus*

(Plourde et al. 2001). Moreover, the presence of early stages of *C. finmarchicus* in the SWGSL in the Summer-Fall suggests that local production of this species might also support *Calanus* spp. biomass in the region (Devine et al. 2017).

Diel vertical migrations (DVM) by various prey had a small effect on their availability to foraging NARW, but had no effect on foraging habitat suitability. *C. hyperboreus*, which has the potential to provide the most energy to NARW, enters diapause in June, with only a very small proportion of the population performing DVM during June and the rest of the summer (Plourde et al. 2003, Plourde et al. 2019).

Our results indicate that the probability of observing suitable NARW foraging habitat in regions shallower than 50 m was extremely low (0.5% in the SWGSL), confirming previous results showing that *Calanus* species and krill abundance is strongly limited at sea floor depths < 100 m (Albouy-Boyer et al. 2016, Plourde et al. 2016). In the SWGSL, suitable habitats were associated to 50-100 m deep areas. In this region, the overwintering vertical distribution of *C. hyperboreus* that were transported in the region as early stages during their active spring period is strongly limited by sea floor depth, resulting in a concentration of *Calanus* biomass close to the sea floor (Plourde et al. 2019). Depth-integrated energy potentially contributed by krill was small, but ranked third in importance for NARW after *C. hyperboreus* and *C. finmarchicus*. The low capture efficiency of NARW feeding on adult krill was inferred from NARW morphology and foraging behaviour (swim speed) and the known avoidance capability of krill. The potential contribution of krill to NARW energy requirements was even lower in the SWGSL. In this region, adult krill abundance is generally low due to limited transport resulting from their extensive DVM and shallow sea floor depth (McQuinn et al. 2015, Maps et al.2013, Plourde et al. 2016, Lavoie et al. 2018).

NARW suitable habitat distribution and persistence in the SWGSL (June-July) and NGSL (August-September) differed between 2006-2010 and 2011-2017, i.e. before and after the observed change in NARW population summer distribution and decrease in calving success (Pettis et al. 2018) and in *Calanus* biomass in the Northwest Atlantic (Sorochan et al. 2019). In 2006-2010, habitats that were suitable for foraging in June-July in the SWGSL were mainly located in the southern half of the region, whereas they were mostly located in the northwest sector of the region and were less persistent also during the 2011-2017 period (Figure 14). In August September in the NGSL, the main change observed between the 2006-2010 and 2011-2017 periods was the presence of suitable habitats west and east of the Jacques-Cartier Strait north of the Anticosti Island in the latter period (Figure 15). Identifying the mechanisms causing these changes was beyond the scope of our study. However, marked interannual variations in *C. hyperboreus* depth-integrated energy were noted in the SWGSL with low values observed more frequently in 2011-2017 than in 2006-2010, a pattern not observed in the NGSL (Figure A.3.1). This region-specific interannual variability in available energy suggest that changes in suitability and persistence in the SWGSL (June-July) and NGSL (August-September) may be driven mainly by a change in bio-physical coupling between C. *hyperboreus* and regional circulation patterns, and not by a change in productivity in deeper regions of the GSL. Overall, the sharp decrease in the potential energy gain by NARW foraging on *Calanus* species in the SWGSL was not compensated by an equivalent increase in energy contribution from other taxa.

## SOURCES OF UNCERTAINTIES

The spatial resolution of zooplankton sampling coverage should be considered as minimal, in particular in the SWGSL during the September Ecosystem surveys. However, the systematic (SWGSL in June) or the stratified-random (NGSL in August, SWGSL in September) sampling designs used for zooplankton sampling that ensure coverage of the entire GSL, are required to for identifying areas hosting high abundance of zooplankton (Plourde et al. 2019). In fact,

Plourde et al. (2019) estimated that 8% of all stations sampled in a similar manner between 1982 and 2014 in the SWGSL, and 2006 and 2014 in the NGSL showed maximum energy density > 20 kJ $m^{-3}$, suggesting that the sampling spatial resolution was sufficient to encompass very high prey densities associated with physical concentration processes typical of known NARW suitable habitats (Baumgartner and Mate 2003). Nevertheless, a larger number of stations that are better distributed would improve our assessment of mesozooplankton distribution and abundance in the region and our ability to estimate seasonal variability.

Statistical models describing the vertical distribution of zooplankton taxa certainly underestimated the density of discrete zooplankton vertical layers that could be formed under particular environmental conditions potentially important for NARW foraging habitats. Statistical models described the average response of the population to the explanatory variables. GAMs for copepods included the effect of sampling depth and the relative sampling depth vs bathymetry, allowing the model to estimate the response of *Calanus* vertical distribution to limiting depth (Krumhansl et al. 2018, Plourde et al. 2019). This was not the case with the simpler statistical models developed for krill because of data limitation. A better model describing krill vertical distribution in various environments could be obtained by analyzing multi-frequency acoustic data in the future.

The limitations of the NARW bio-energetic foraging model and its comparison with previous studies were reported in Gavrilchuk et al. (2020). We investigated the range of possible suitable habitats by using the same approach as Gavrilchuk et al (2020) which consist of applying the model using the parameters that resulted in minimum and maximum $E_{net}$ for adult female NARW in three different reproductive states. Some parameters were based on individual variability such as the mouth area, while other parameters such as prey energy density depended on the environment. While these parameters capture the “known” uncertainty, some uncertainty such as the effect of climate change and NARW behaviour could not be accounted for.

Given the health decline in all NARW demographic groups over the past three decades, and the likelihood that females successfully reproducing being those that were healthier the previous year (Rolland et al. 2016), it may be that resting females in poor health may require more energy than is currently estimated in the model (Rolland et al. 2016). Under this scheme, our choice of using an intermediate scenario, i.e. pregnant females and a set of model parameters resulting in an averaged $E_{net}$, with the bio-energetic model for our analyses, could be representative of the metabolic needs of both pregnant, and resting females in poor condition, a situation more likely during the recent period of distributional change and low calving rate (Pettis et al. 2018). Our bio-energetic modelling approach did not take into account species-specific changes in zooplankton individual body size and energy content resulting from a warmer environment (McKinstry et al. 2013, Sorochan et al. 2019). Such changes have been observed in the GSL and particularly in the SWGSL, where *C. finmarchicus* body size in the summer was smaller after 2012 relative to the previous decades (Sorochan et al. 2019). Although these changes are of smaller amplitude than the interannual variability in abundance, they could nonetheless affect our estimates of biomass and energy of *Calanus* species available to NARW.

Foraging behavior of NARW represents further uncertainty in the parameters used to calculate habitat suitability . Southern right whales have been observed feeding on *Euphausia superba* (Hamner et al. 1988) at a ramming speed of ~4 m/s, which is higher than the 1 m/s used in our model. Instead of assuming a change in the behaviour (parameters affecting $E_{out}$), the capture efficiency was considered (parameter affecting $E_{in}$). This capture efficiency assumes that NARW have a filtration efficiency similar to a 333µm net without strobe and towed at the same speed as a foraging NARW. This does not take into account possible adaptation in behaviour such as suction-feeding, which may be exhibited by NARW.

In conclusion, *C. hyperboreus* represented the main source of energy available to NARW in the GSL. *C. finmarchicus* provided 5-10 times less energy than *C. hyperboreus* depending on the region and season, with its contribution increasing through Summer in the SWGSL. *Pseudocalanus spp.*, *Temora spp.* and krill provided negligible amounts of energy to NARW because of their small body size and high swimming capacities, respectively. Our results also revealed an extremely low probability (0.5% in the SWGSL) for a suitable habitat to occur in regions shallower than 50 m. Finally, most of the habitats suitable for foraging NARW in June-July were located in the SWGSL. In August-September, habitat suitability declined in the SWGSL and increased in the NGSL, making the NGSL a region with more suitable habitats for NARW.

## REFERENCES CITED


Albouy-Boyer, S., Plourde, S., Pepin, P., Johnson, C.L., Lehoux, C., Galbraith, P.S., Hebert, D., Lazin, G., and Lafleur, C. 2016. Habitat modelling of key copepod species in the Northwest Atlantic Ocean based on the Atlantic Zone Monitoring Program. J. Plank. Res., 38(3), 589-603.

Baumgartner, M.F., and Mate, B.R. 2003. Summertime foraging ecology of North Atlantic right. Mar. Ecol. Prog. Ser. 264: 123–135.

Baumgartner, M. F., Cole, T. V. N., Campbell, R. G., Teegarden, G. J., and Durbin, E. G. 2003. Associations between North Atlantic right whales and their prey, *Calanus finmarchicus*, over diel and tidal time scales. Mar. Ecol. Prog. Ser., 264: 155–166.

Baumgartner, M. F., Mayo, C. A., and Kenney, R. D. 2007. Enormous carnivores, microscopic food, and a restaurant that's hard to find. The urban whale: North Atlantic right whales at the crossroads. Harvard University Press, Cambridge, MA, 138-171.

Baumgartner, M. F., Wenzel, F. W., Lysiak, N. S. J., and Patrician, M. R. 2017. North Atlantic right whale foraging ecology and its role in human-caused mortality. Mar. Ecol. Prog. Ser., 581: 165–181.

Bivand, R. and Lewin-Koh, N. 2018. maptools: Tools for Handling Spatial Objects. R package version 0.9-4.

Brennan, C.E., Maps, F., Gentleman, W.C., Plourde, S., Lavoie, D., Chassé, J., Lehoux, C., Krumhansl, K.A., and Johnson, C.L. 2019. How transport shapes copepod distributions in relation to whale feeding habitat: Demonstration of a new modelling framework. Prog. Oceanogr. 171: 1–21.

Brey, T., Müller-Wiegmann, C., Zittier, Z. M. C., and Hagen, W. 2010. Body composition in aquatic organisms - A global data bank of relationships between mass, elemental composition and energy content. J. Sea Res. 64: 334–340.

Collet, R. 1909. A few notes on the whale *Balaena glacialis* and its capture in recent years in the North Atlantic by Norwegian whalers. Proc. Zool. Soc. Lond. 7: 91-98.

Conover, R. J., and Huntley, M. 1991. Copepods in ice-covered seas—distribution, adaptations to seasonally limited food, metabolism, growth patterns and life cycle strategies in polar seas. J. Mar. Syst., 2(1-2), 1-41.

Davies, K. T., Ryan, A., and Taggart, C. T. 2012. Measured and inferred gross energy content in diapausing Calanus spp. in a Scotian shelf basin. J. Plank. Res., 34(7), 614-625.

Devine, L., Scarratt, M., Plourde, S., Galbraith, P.S., Michaud, S., and Lehoux, C. 2017. Chemical and Biological Oceanographic Conditions in the Estuary and Gulf of St. Lawrence during 2015. DFO Can. Sci. Advis. Sec. Res. Doc. 2017/034. v + 48 pp.

DFO. 2019. Review of North Atlantic right whale occurrence and risk of entanglements in fishing gear and vessel strikes in Canadian waters. DFO Can. Sci. Advis. Sec. Sci. Advis. Rep. 2019/028.

Dunn, O. J. 1964. Multiple comparisons using rank sums. Technometrics 6, 241–252.

Galbraith, P.S., Chassé, J., Caverhill, C., Nicot, P., Gilbert, D., Lefaivre, D. and Lafleur, C. 2018. Physical Oceanographic Conditions in the Gulf of St. Lawrence during 2017. DFO Can. Sci. Advis. Sec. Res. Doc. 2018/050. v + 79 p.

Gavrilchuk, K., Lesage, V., Fortune, S. , Trites, A.W., and Plourde, S. 2020. A mechanistic approach to predicting suitable foraging habitat for North Atlantic right whales in the Gulf of St. Lawrence, Canada. DFO Can. Sci. Advis. Sec. Res. Doc. 2020/034. iv + 47 p.

Gräler, B., Pebesma, E. and Heuvelink G. 2016. Spatio-Temporal Interpolation using gstat. R J. 8(1), 204-218.

Hay, S. J., Evans, G. T., and Gamble, J. C. (1988). Birth, growth and death rates for enclosed populations of calanoid copepods. J. Plank. Res., 10(3), 431-454.

Hamner, W. M., Stone, G. S., and Obst, B. S. 1988. Behavior of southern right whales, *Eubalaena australis*, feeding on the Antarctic krill, *Euphausia superba*. Fish. Bull., 86: 143–150.

Hijmans, R.J. 2018. raster: Geographic Data Analysis and Modeling. R package version 2.7-15.

Kenney, R. D., Hyman, M. A., Owen, R. E., Scott, G. P., and Winn, H. E. 1986. Estimation of prey densities required by western North Atlantic right whales. Mar. Mamm. Sci. 2(1), 1-13.

Kenney, R. D., Winn, H. E., and Macaulay, M. C. 1995. Cetaceans in the Great South Channel, 1979–1989: right whale (*Eubalaena glacialis*). Cont. Shelf Res. 15(4-5), 385-414.

Kraus, SD, et Prescott, J. H. 1982. “The North Atlantic Right Whale (*Eubalaena Glacialis*) in the Bay of Fundy, 1981, with Notes on the Distribution, Abundance, Biology and Behavior.”

Krzystan, A.M., Gowan, T.A., Kendall, W.L., Martin, J., Ortega-Ortiz, J.G., Jackson, K., Knowlton, A.R., Naessig, P., Zani, M., Schulte, D.W., and Taylor, C.R. 2018. Characterizing residence patterns of North Atlantic right whales in the southeastern USA with a multistate open robust design model. Endanger. Species Res. 36:279–295.

Krumhansl, K. A., Head, E. J. H., Pepin, P., Plourde, S., Record, N. R., Runge, J. A., and Johnson, C. L. 2018. Environmental drivers of vertical distribution in diapausing Calanus copepods in the Northwest Atlantic. Prog. Oceanogr. 162: 202–222.

Lavoie, D., Chassé, J., Simard, Y., Lambert, N., Galbraith, P. S., Roy, N., and Brickman, D. 2016. Large-scale atmospheric and oceanic control on krill transport into the St. Lawrence Estuary evidenced with three-dimensional numerical modelling. Atmosphere-Ocean, 54(3), 299-325.

Maps, F., Plourde, S., and Zakardjian, B. 2010. Control of dormancy by lipid metabolism in *Calanus finmarchicus*: A population model test. Mar. Ecol. Prog. Ser. 403: 165–180. doi:10.3354/meps08525.

Maps, F., Zakardjian, B., Plourde, S., and Saucier, F.J. 2011. Modeling the interactions between the seasonal and diel migration behaviors of *Calanus finmarchicus* and the circulation in the Gulf of St. Lawrence (Canada). J. Mar. Syst., 88: 183-202, doi:10.1016/j.jmarsys.2011.04.004

Maps, F., Plourde, S., Lavoie, D., McQuinn, I., and Chassé, J. 2013. Modelling the influence of daytime distribution on the transport of two sympatric krill species (*Thysanoessa raschii* and *Meganyctiphanes norvegica*) in the Gulf of St Lawrence, eastern Canada. ICES J. Mar. Sci., 71 (2): 282-292, doi:10.1093/icesjms/fst021

Mayo, C.A., and Marx, M.K. 1990. Surface Foraging Behavior of the North Atlantic Right Whale Eubalaena -Glacialis and Associated Zooplankton Characteristics. Can. J. Zool. 68(10): 2214–2220. doi:10.1139/z90-308.

Mayo, C.A., Letcher, B.H., and Scott, S. 2001. Zooplankton flitering efficiency of the baleen of a North Atlantic right whale, *Eubalaena glacialis*. J. Cetacean Res. Manage. Special Issue 2: 225-229.

McKinstry, C.A.E., Westgate, A.J., and Koopman, H.N. 2013. Annual variation in the nutritional value of stage V *Calanus finmarchicus*: Implications for right whales and other copepod predators. Endanger. Species Res. 20(3): 195–204.

McQuinn, I.H., Dion, M. and St. Pierre, J.-F. 2013. The acoustic multifrequency classification of two sympatric euphausiid species (*Meganyctiphanes norvegica* and *Thysanoessa raschii*), with empirical and SDWBA model validation. ICES J. Mar. Sci., 70(3), pp.636–649.

McQuinn, I. H., Plourde, S., St. Pierre, J. F., and Dion, M. 2015. Spatial and temporal variations in the abundance, distribution, and aggregation of krill (*Thysanoessa raschii* and *Meganyctiphanes norvegica*) in the lower estuary and Gulf of St. Lawrence. Prog. Oceanogr., 131: 159–176.

McQuinn, I.H., Gosselin, J.-F., Bourassa, M.-N., Mosnier, A., St-Pierre, J.-F., Plourde, S., Lesage, V., and Raymond, A. 2016. The spatial association of blue whales (*Balaenoptera musculus*) with krill patches (Thysanoessa spp. and *Meganyctiphanes norvegica*) in the estuary and northwestern Gulf of St. Lawrence. DFO Can. Sci. Advis. Sec. Res. Doc. 2016/104. iv + 19 p.

Michaud, J., and Taggart, C. T. 2007. Lipid and gross energy content of North Atlantic right whale food, *Calanus finmarchicus*, in the Bay of Fundy. Endang. Species Res. 3(1): 77-94.

Murison, LD. 1986. Zooplankton Distributions and Feeding Ecology of Right Whales (*Eubalaena Glacialis Glacialis*) in the Outer Bay of Fundy, Canada. University of Guelph, Guelph, Canada.

Murison, L D, and Gaskin, D. E. 1989. The Distribution of Right Whales and Zooplankton in the Bay of Fundy, Canada. Can. J. Zool. 67 (6): 1411–20. doi.org/10.1139/z89-200.

Nichols, J. H., and Thompson, A. B. 1991. Mesh selection of copepodite and nauplius stages of four calanoid copepod species. J. Plank. Res., 13: 661–671.

Nousek McGregor, A.E. 2010. “The Cost of Locomotion in North Atlantic Right Whales *Eubalaena Glacialis*.” Duke University.

Pebesma, E.J. 2004. Multivariable geostatistics in S: the gstat package. Comput. Geosci., 30: 683-691.

Pettis, H.M., Pace, R.M. III, Schick, R.S., and Hamilton, P.K. 2018. North Atlantic Right Whale Consortium annual report card. Amended Report to the North Atlantic Right Whale Consortium, October 2017.

Plourde, S., Joly, P., Runge, J. A., Zakardjian, B. and Dodson, J. J. 2001. Life cycle of *Calanus finmarchicus* in the lower St. Lawrence Estuary: The imprint of circulation and late timing of the spring phytoplankton bloom. Can. J. Fish. Aquat. Sci. 58, 647-658.

Plourde, S., Joly P., Runge, J., Dodson J., and Zakardjian, B. 2003. Life cycle of *Calanus hyperboreus* in the lower St. Lawrence Estuary and its relationship to local environmental conditions, Mar. Ecol. Prog. Ser .255: 219–233.

Plourde, S., McQuinn, I.H., Maps, F., St-Pierre, J.-F., Lavoie, D., and Joly, P. 2014. Daytime depth and thermal habitat of two sympatric krill species in response to surface salinity variability in the Gulf of St Lawrence, eastern Canada. ICES J. Mar. Sci. 71(2): 272–281.

Plourde, S., Lehoux, C., McQuinn, I.H., and Lesage, V. 2016. Describing krill distribution in the western North Atlantic using statistical habitat models. DFO Can. Sci. Advis. Sec. Res. Doc. 2016/111. v + 34 p.

Plourde, S., Lehoux, C., Johnson, C. L., Perrin, G., and Lesage, V. 2019. North Atlantic right whale (*Eubalaena glacialis*) and its food: (I) a spatial climatology of *Calanus* biomass and potential foraging habitats in Canadian waters. J. Plank. Res. doi:10.1093/plankt/fbz024

Rolland, R., Schick, R., Pettis, H., Knowlton, A., Hamilton, P., Clark, J., and Kraus, S. 2016. Health of North Atlantic right whales Eubalaena glacialis over three decades: from individual health to demographic and population health trends. Mar. Ecol. Prog. Ser. 542: 265–282.

Sameoto, D., Cochrane, N., and Herman, A. 1993. Convergence of acoustic, optical, and net-catch estimates of euphausiid abundance: use of artificial light to reduce net. Can. J. Fish. Aquat. Sci., 50(2), 334-346.

Simard, Y., and Sourisseau, M. 2009. Diel changes in acoustic and catch estimates of krill biomass. ICES J. Mar. Sci., 66(6), 1318-1325.

Sorochan, K. A., Plourde, S., Morse, R., Pepin, P., Runge, J., Thompson, C., and Johnson, C. L. 2019. North Atlantic right whale (*Eubalaena glacialis*) and its food: (II) interannual variations in biomass of Calanus spp. on northwest Atlantic shelves. J. Plank. Res., 41(5), 687-708.

Thorsten, P. 2018. PMCMRplus: Calculate Pairwise Multiple Comparisons of Mean Rank Sums Extended. R package version 1.4.1.

van der Hoop, J.M., Nousek-McGregor, A.E., Nowacek, D.P., Parks, S.E., Tyack, P., and Madsen, P.T. 2019. Foraging rates of ram-filtering North Atlantic right whales. Funct. Ecol. 33: 1290–1306.

Watkins, W. A, and Schevill, W.E. 1976. “Right Whale Feeding and Baleen Rattle.” J. Mammal. 57 (1): 58–66.

Wiebe, P. H., Ashjian, C. J., Gallager, S. M., Davis, C. S., Lawson, G. L., and Copley, N. J. 2004. Using a high-powered strobe light to increase the catch of Antarctic krill. Mar. Biol. 144(3), 493-502.

Wiebe, P. H., Lawson, G. L., Lavery, A. C., Copley, N. J., Horgan, E., and Bradley, A. 2013. Improved agreement of net and acoustical methods for surveying euphausiids by mitigating avoidance using a net-based LED strobe light system. ICES J. Mar. Sci, 70: 650–664.

Wishner, K., Durbin, E., Durbin, A., Macaulay, M., Winn, H., and Kenney, R. 1988. Copepod patches and right whales in the Great South Channel off New England. Bull. Mar. Sci. 43(3): 825-844.

# TABLES

*Table 1. Individual biomass (dry weight, mg), energetic density (kJ $g^{-1}$), fraction of abundance filtered by NARW baleen, and fraction of biomass capture NARW of late stages of copepods and adult krill. Individual biomass is stage and month-dependent. See cited references for details.*

| Species | Individual biomass (mg) | Energetic content (kJ $g^{-1}$) Mean ± sd | Foraging efficiency | |
|---|---|---|---|---|
| | | | Filtering efficiency 200/333µm[8] | Capture efficiency D/N[9] |
| ***C. finmarchicus/glacialis*** | 0.2-0.3[1] | 27.9±5.0[6] | 1 | 1 |
| ***C. hyperboreus*** | 1.7-2.2[2] | 27.9±5.0[6] | 1 | 1 |
| ***Pseudocalanus spp.*** | 0.01-0.02[3] | 22.73±0.65[7] | 0.5/1 | 1 |
| ***Temora spp.*** | 0.01[4] | 19.72±1.05[7] | 0.5/1 | 1 |
| ***M. norvegica*** | Calculated for mean length in the stratum[5] | 25.03±3.27[7] | 1/1 | 0.17/0.27 |
| ***T. raschii*** | | 22.68±2.92[7] | 1/1 | 0.035/0.22 |

[1] Maps et al. 2010, 2011. [2] Plourde et al. 2003. [3] Conover and Huntley 1991. [4] Hay et al. 1988. [5] McQuinn et al. 2015. [6] Davies et al. 2012. [7] Brey et al. 2010. [8] Nichols and Thompson, 1991. [9] St-Pierre and McQuinn DFO, unpublished data.

*Table 2. GAMs results fitted using stratified vertical samples in the Gulf of St Lawrence for Calanus finmarchicus / glacialis (C. fin/glac), Calanus hyperboreus (C. hyp), Pseudocalanus spp. (Pseudo) and Temora spp. The deviance explained by the model (DEV) is presented along with the formula of the selected models. Z is the station depth and %Z is the proportion of station depth sampled. Cross-validation was repeated 10 times with 30% of the station for model evaluation and 70% for model calibration. The fit of the model is evaluated with the mean Spearman correlation coefficient (ρ) after 10 iterations and the linear regression (mean intercept= $\beta_0$, mean slope= $\beta_1$ and the adjusted $R^2$ with its standard deviation) between observed and predicted values.*

| Species | Season | D/N | N | DEV (%) | formula | Cross-validation | | | |
|---|---|---|---|---|---|---|---|---|---|
| | | | | | | ρ | $\beta_0$ | $\beta_1$ | $R^2$ (sd) |
| *C. fin/glac* | Jun-Jul | D | 150 | 97 | %Z*** + %Z *x* Z *** + Z** | 0.9 | 0.07 | 0.89 | 0.82 (0.12) |
| *C. fin/glac* | Jun-Jul | N | 72 | 95 | %Z*** + Z*** | 0.75 | 0.19 | 0.68 | 0.61 (0.3) |
| *C. fin/glac* | Aug-Sep | D | 156 | 96 | %Z*** | 0.93 | 0.08 | 0.82 | 0.87 (0.07) |
| *C. fin/glac* | Aug-Sep | N | 94 | 94 | %Z*** | 0.84 | 0.12 | 0.77 | 0.71 (0.12) |
| *C. hyp* | June-Jul | D | 150 | 98 | %Z*** + %Z *x* Z** + Z*** | 0.93 | 0.03 | 0.96 | 0.87 (0.07) |
| *C. hyp* | June-Jul | N | 72 | 96 | %Z*** + Z*** | 0.78 | 0.13 | 0.77 | 0.65 (0.3) |
| *C. hyp* | Aug-Sep | - | 250 | 98 | %Z*** + Z* | 0.79 | 0.12 | 0.81 | 0.68 (0.33) |
| *Pseudo* | - | D | 330 | 90 | %Z*** + Z*** | 0.85 | 0.15 | 0.7 | 0.72 (0.08) |
| *Pseudo* | - | N | 211 | 93 | %Z*** + Z*** | 0.82 | 0.14 | 0.74 | 0.68 (0.08) |
| *Temora* | - | D | 143 | 92 | %Z*** + %Z *x* Z*** + Z*** | 0.87 | 0.15 | 0.76 | 0.76 (0.14) |
| Temora | - | N | 74 | 93 | %Z*** + Z*** | 0.89 | 0.1 | 0.87 | 0.79 (0.13) |

*Table 3. Number of samples (N) and equations describing the vertical distribution of krill in the Gulf of St Lawrence. y is the cumulated abundance (%) from top to bottom and x is the sampled depth (m).*

| | N | *M.norvegica* | $R^2$ | *Thysanoessa spp.* | $R^2$ |
|---|---|---|---|---|---|
| NWGSL and SWGSL- Day | 54 | $y = \frac{99.4575}{1 + e^{\left[\frac{-(x-122.2528}{18.5634}\right]}}$ | 0.84 | $y = \frac{99.8205}{1 + e^{\left[\frac{-(x-92.4412}{21.2336}\right]}}$ | 0.81 |
| NEGSL - Day | 36 | $y = \frac{103.2590}{1 + e^{\left[\frac{-(x-181.0455}{22.6696}\right]}}$ | 0.89 | $y = \frac{102.7617}{1 + e^{\left[\frac{-(x-143.6922}{23.4395}\right]}}$ | 0.94 |
| GSL - Nuit | 72 | $y = 104.1420 \times \frac{x}{20.8966 + x}$ | 0.66 | $y = 109.0355 \times \frac{x}{19.5252 + x}$ | 0.69 |

*Table 4. Sensitivity of model predictions to parameter uncertainty. The percentage of cells with at least one year with a positive $E_{net}$ (% cells) and for these cells the mean and standard deviation of the percentage of years with a positive $E_{net}$ (% years) was calculated for each run that considered the energy requirement of resting, pregnant or lactating females and considering the uncertainty around each parameters that results in the minimum, mean or maximum $E_{net}$. The $E_{net}$min is given by the combination of parameters that gives the minimum $E_{in}$ and maximum $E_{out}$. The $E_{net}$mean is given by the combination of parameters that give the mean $E_{in}$ and $E_{out}$. The $E_{net}$max is given by the combination of parameters that give the maximum $E_{in}$ and the minimum $E_{out}$. All runs used the eergy gained by all copepod taxa combined and excluded krill.*

| | | NGSL | | | | SWGSL | | | |
|---|---|---|---|---|---|---|---|---|---|
| | | June July | | August September | | June July | | August September | |
| | | % cells | % years | % cells | % years | % cells | % years | % cells | % years |
| Resting | $E_{net}$min | 0.00 | - | 3.62 | 9.24 ± 2.62 | 10.94 | 9.42 ± 3.69 | 0.00 | - |
| | $E_{net}$mean | 1.49 | 8.33 ± 0.00 | 19.15 | 9.91 ± 4.05 | 41.64 | 17.93 ± 10.00 | 3.08 | 8.33 ± 0.00 |
| | $E_{net}$max | 2.23 | 10.19 ± 3.67 | 57.40 | 12.02 ± 5.09 | 59.96 | 28.49 ± 16.04 | 22.42 | 13.03 ± 4.22 |
| Pregnant | $E_{net}$min | 0.00 | - | 0.00 | - | 2.05 | 8.70 ± 1.74 | 0.00 | - |
| | $E_{net}$mean | 0.25 | 8.33 ± 0.00 | 11.07 | 9.48 ± 3.54 | 23.93 | 11.99 ± 6.20 | 0.00 | - |
| | $E_{net}$max | 1.73 | 8.33 ± 0.00 | 37.06 | 10.79 ± 4.54 | 51.96 | 24.03 ± 14.16 | 8.24 | 8.44 ± 0.96 |
| Lactating | $E_{net}$min | 0.00 | - | 0.00 | - | 0.00 | - | 0.00 | - |
| | $E_{net}$mean | 0.00 | - | 0.00 | - | 0.44 | 8.33 ± 0.00 | 0.00 | - |
| | $E_{net}$max | 0.00 | - | 3.56 | 8.33 ± 0 | 7.74 | 9.10 ± 3.51 | 0.00 | - |

## FIGURES

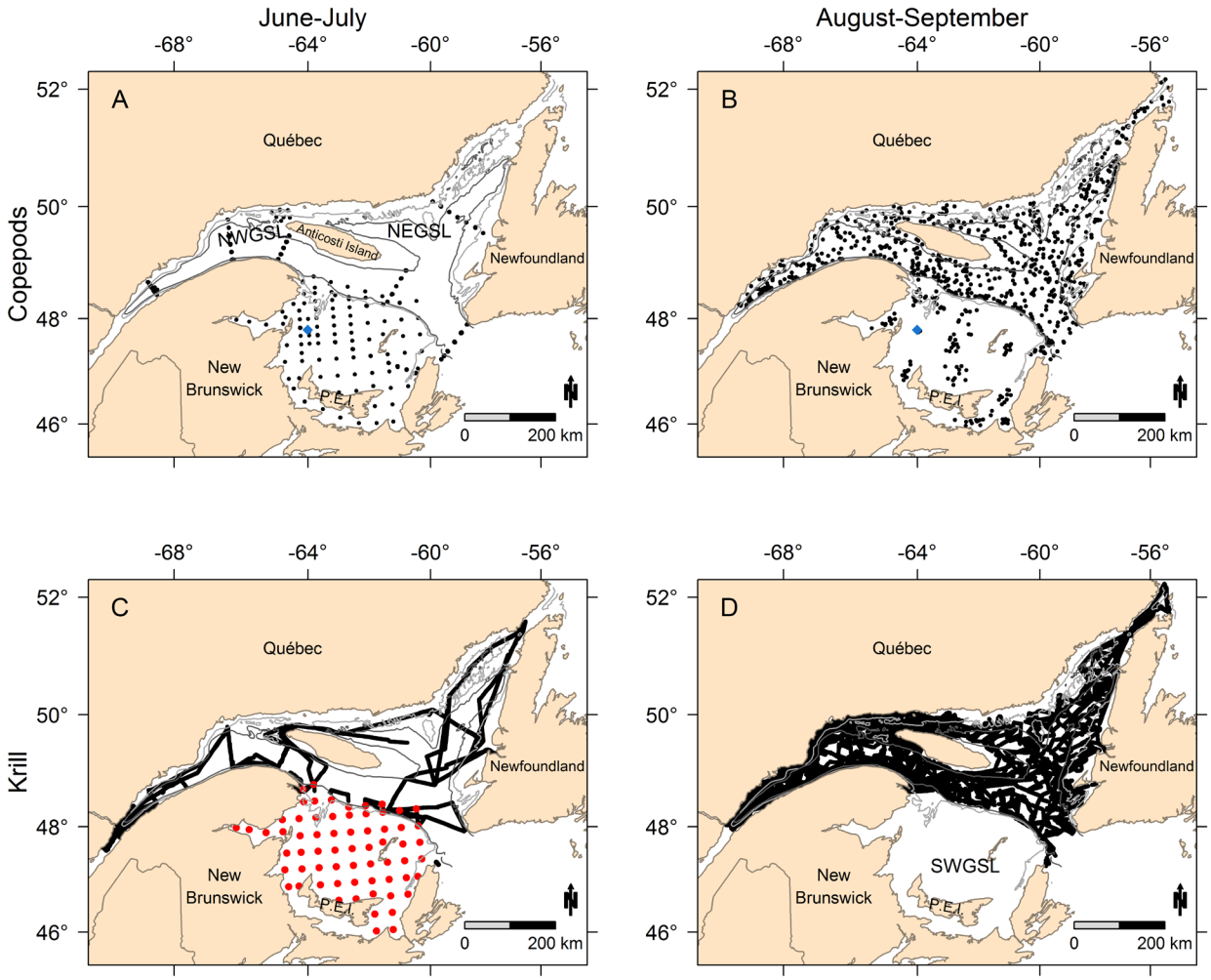


*Figure 1. Stations sampled in June-July (A,C) and August-September (B, D) using different types of net for the copepods (A, B) and multi-frequency acoustics (black cruise tracks) or bongo (red circles) for krill (C,D). The blue diamond in A and B indicate the position of the Shediac station. All maps are projected using the Lambert Conformal Conic projection. The dark grey and pale grey lines represent the 200 m and 100 m isobaths respectively. NWGSL, NEGSL and SWGSL represent the northwest, northeast and southwest Gulf of St. Lawrence respectively. P.E.I = Prince Edward Island.*

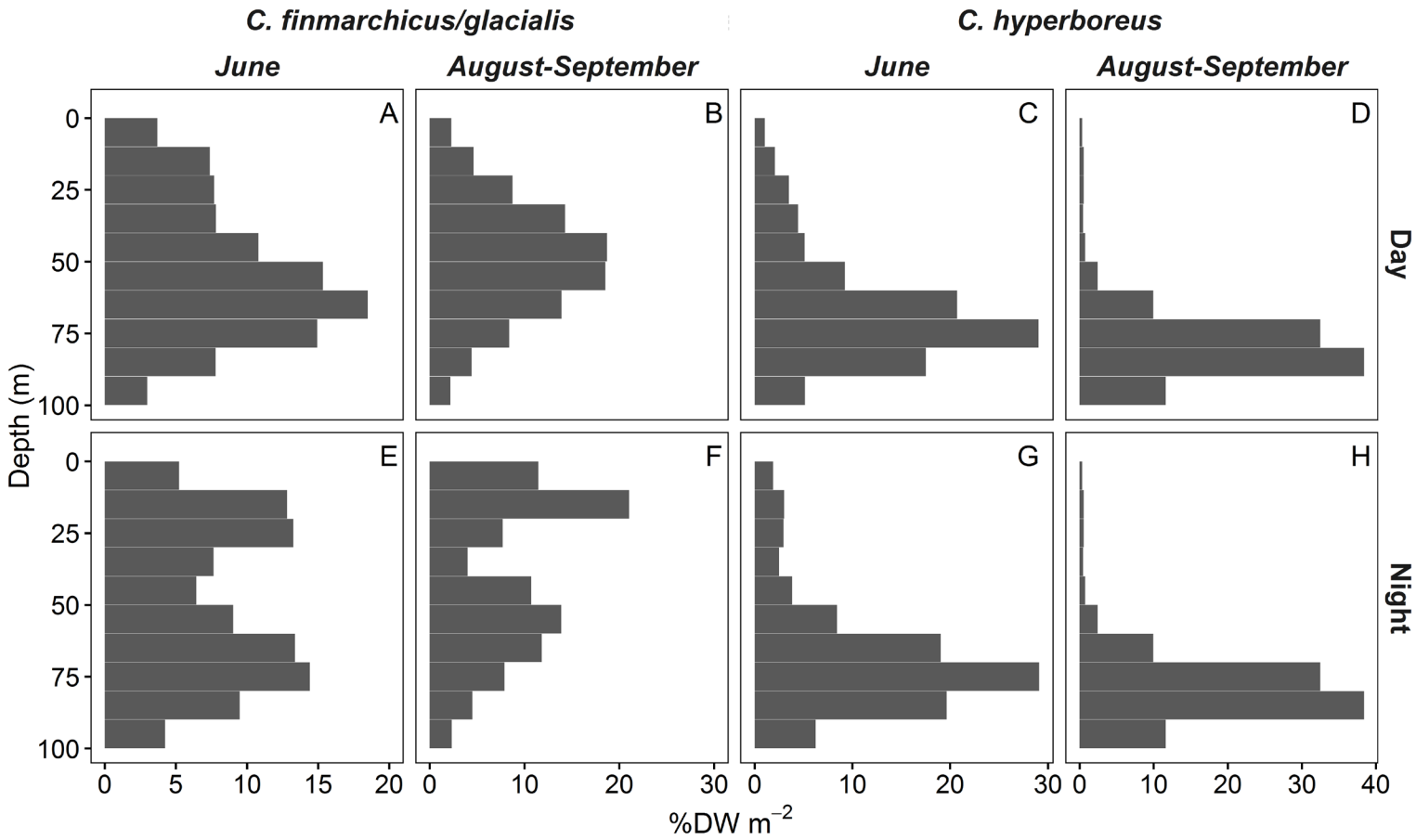


*Figure 2. Predicted percentage in each 10-m bins of the depth-integrated biomass (%DW m$^{-2}$) at a station of 100 m for Calanus finmarchicus/glacialis (A,B,E,F) and Calanus hyperboreus (C,D,G,H) in June (A,C,E,G) and August-September (B,D,F,H) during the day (A-D) and night (E-H). Predictions were made with GAMs. See Table 2 and Appendix 2 for GAMs results.*

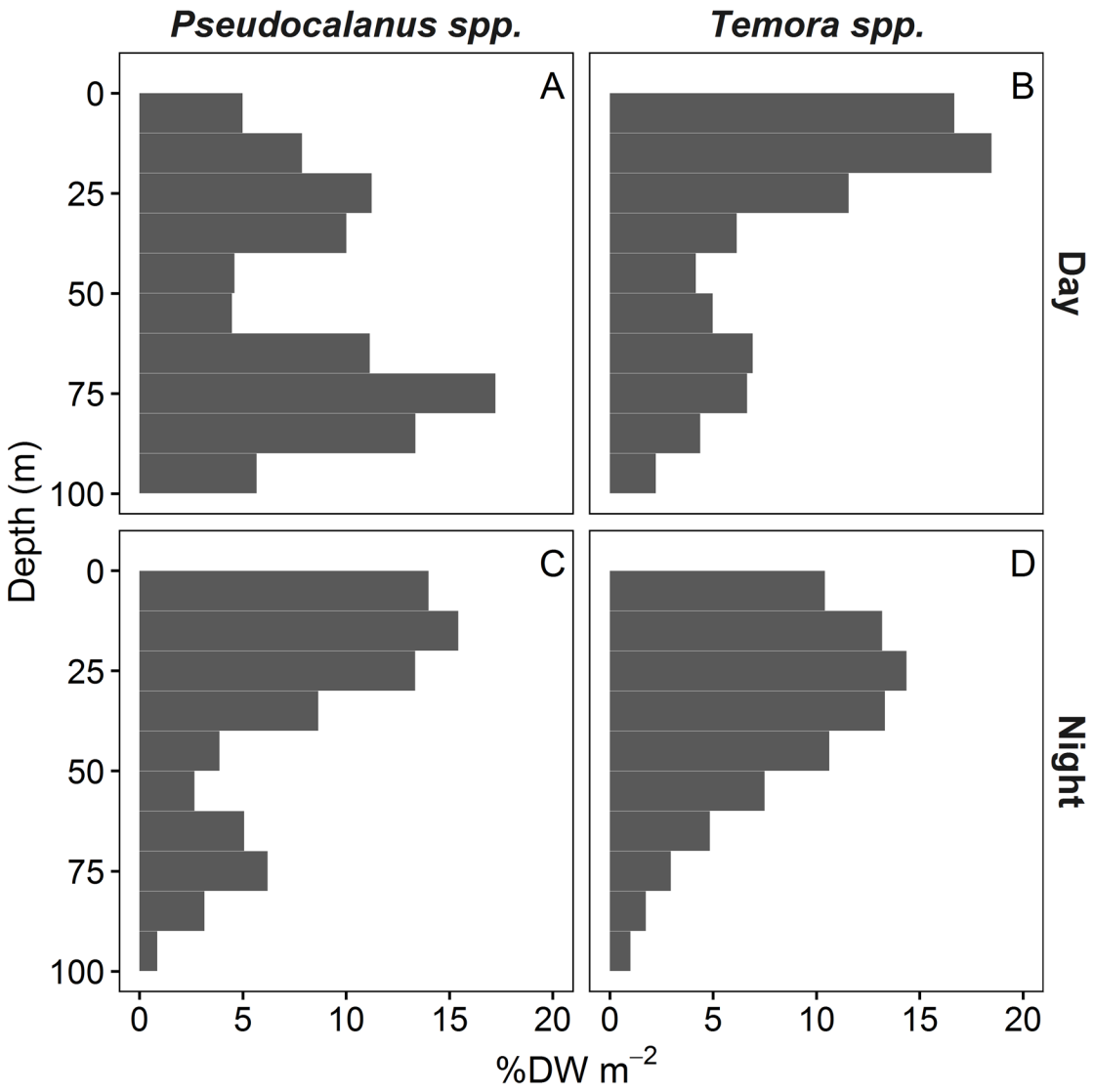


*Figure 3. Predicted percentage in each 10-m bins of the depth-integrated biomass (%DW m$^{-2}$) at a station of 100 m for Pseudocalanus spp. (A, C) and Temora spp. (B, D) during the day (A, B) and the night (C, D). Predictions were made with GAMs. See Table 2 and Appendix 2 for GAMs results.*

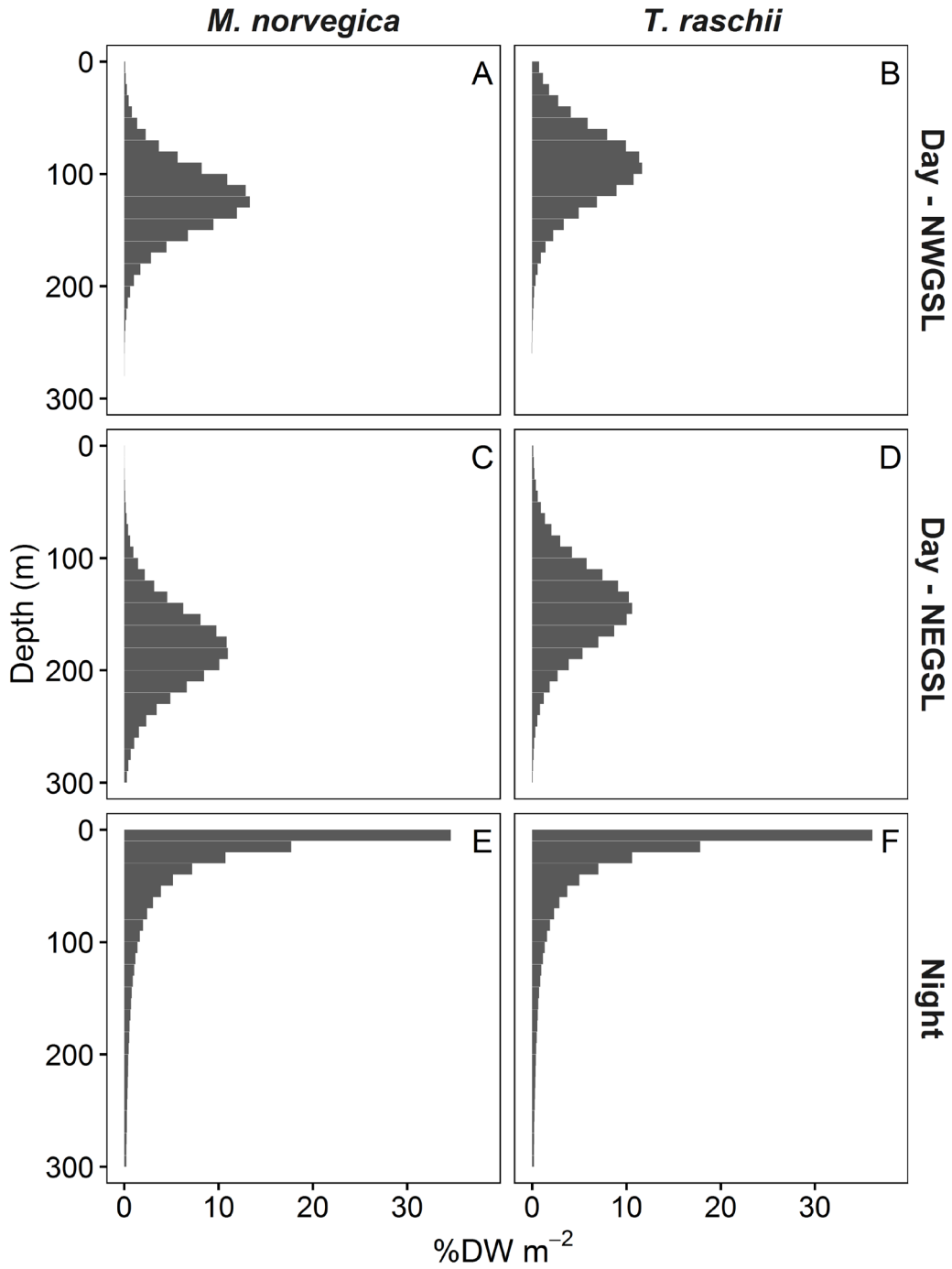


*Figure 4. Predicted percentage in each 10-m bins of the depth-integrated biomass (%DW $m^{-2}$) at a station of 300 m for of M. norvegica (A,C,E) and T. raschii (B,D,F) during the day in the Northwest Gulf of St Lawrence (NWGSL: A, B) and the Northeast Gulf of St Lawrence (NEGSL: C, D) and during the night in both regions (E,F). Predictions were made with equations in Table 3. The vertical distribution of the NWGSL is applied to the SWGSL.*

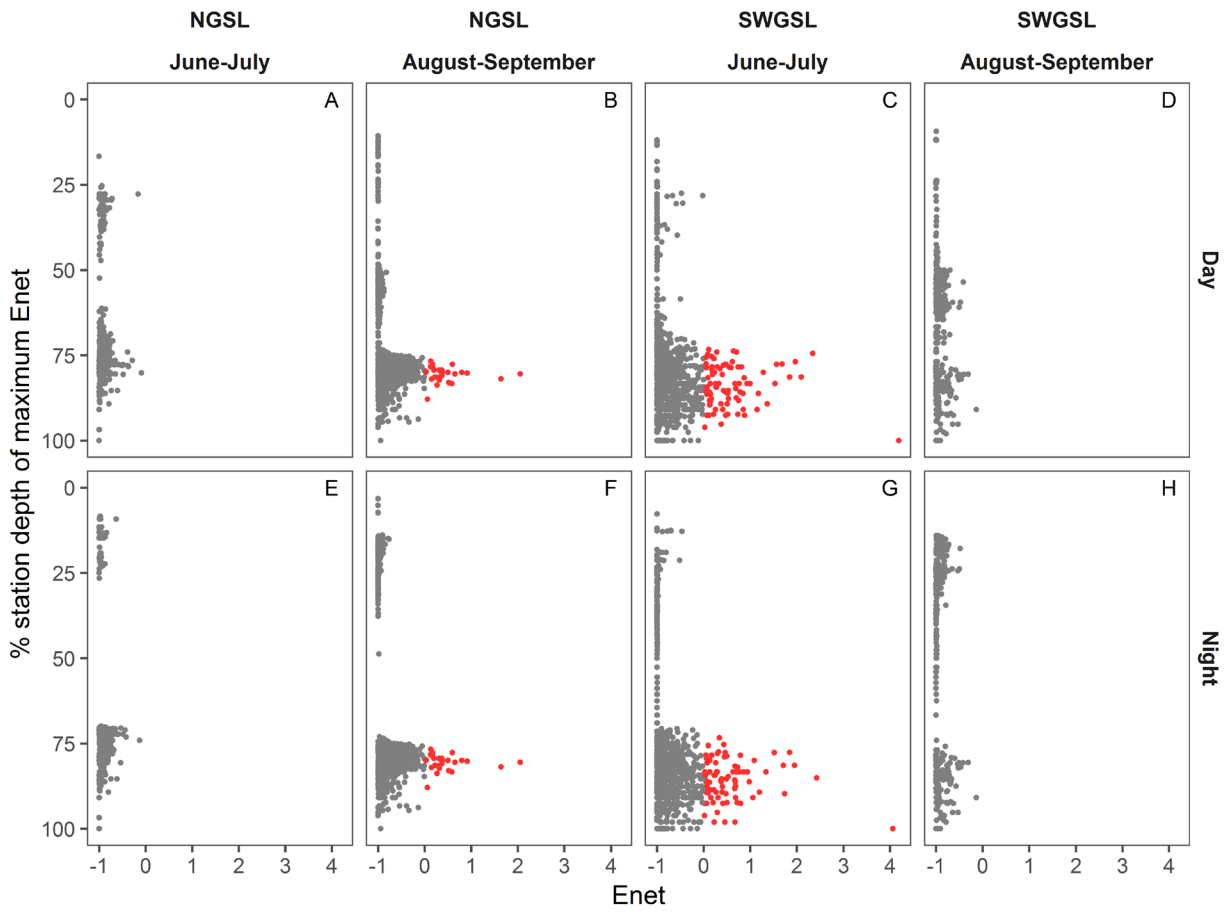


*Figure 5. Layer targeted by pregnant whales feeding on copepods expressed in percentage of stations depth (Depth of maximum $E_{net}$ / Station depth) and the corresponding $E_{net}$ for each stations sampled between 2006 and 2017 showing the effect of feeding on copepods during the day (A-D) or night (E-H) in the NGSL (A,B,E,F) and the SWGSL (C,D,G,H) in June-July (A,C,E,G) and August-September (B,D,F,H). Red circles represent suitable habitat ($E_{net}$ >=0).*

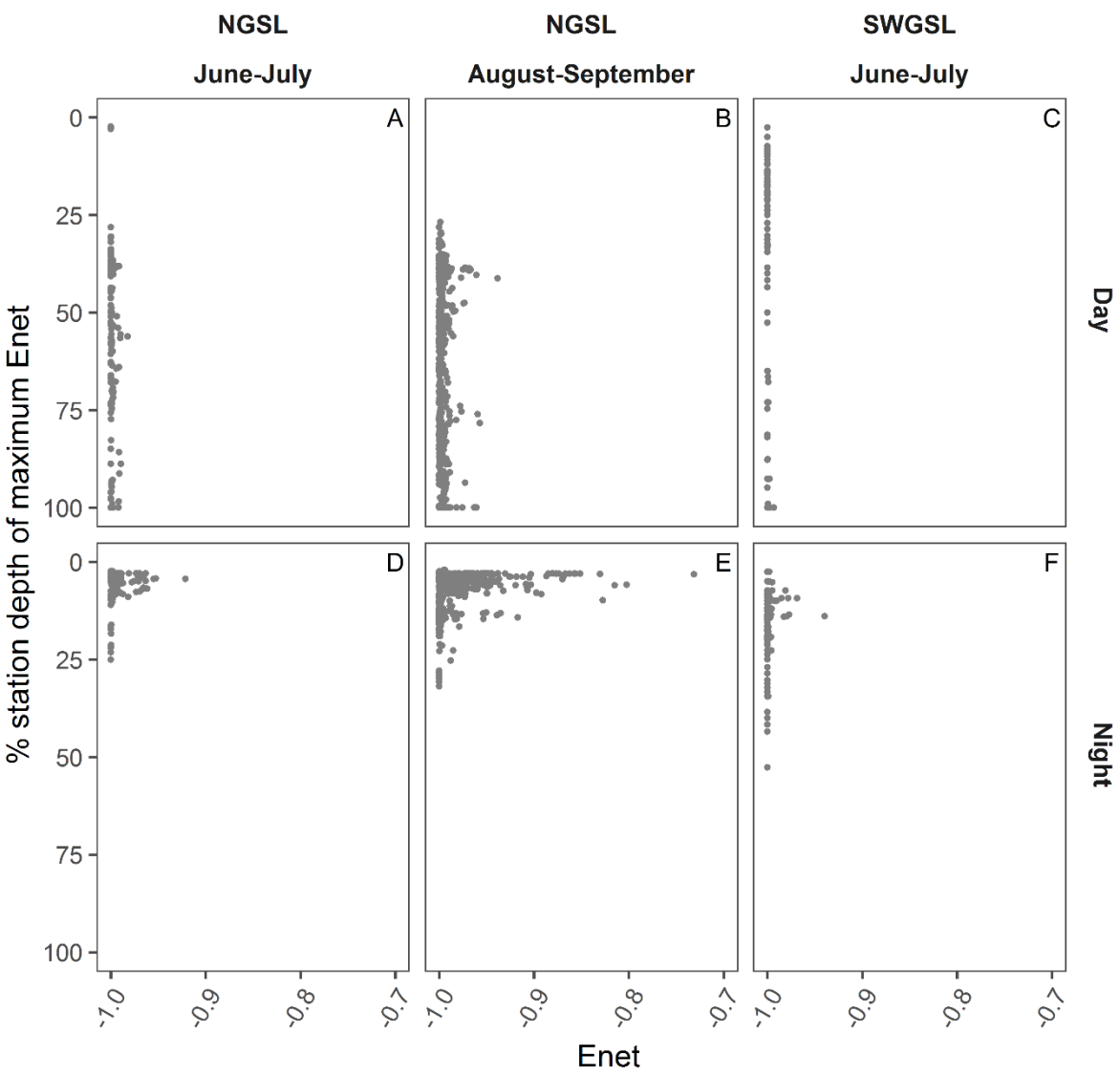


*Figure 6. Layer targeted by pregnant whales feeding on krill expressed in percentage of stations depth (Depth of maximum $E_{net}$ / Station depth) and the corresponding $E_{net}$ for each stations sampled between 2006 and 2017 showing the effect of feeding on krill during the day (A-D) or night (E-H) in the NGSL (A,B,D,E) and the SWGSL (C,F) in June-July (A,C,D,F) and August-September (B,E). Grey circles represent unsuitable habitat ($E_{net}$ <0). Krill stations were 500m-bins of the cruise track that were within 500 m of copepods stations.*

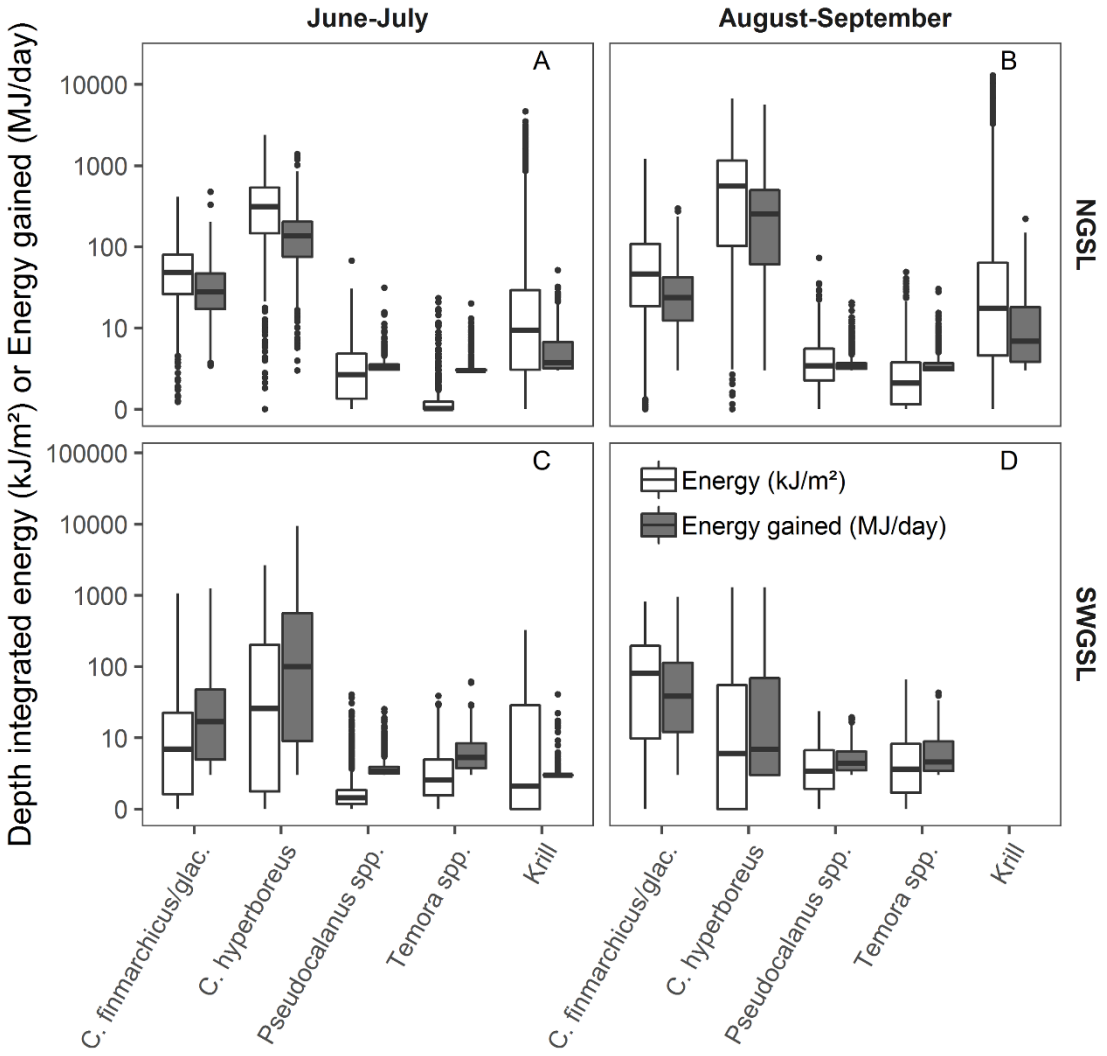


*Figure 7. Depth integrated energy (kJ/m², white) and energy gained by pregnant whales at depth of maximum $E_{net}$ (MJ/day, grey) when feeding on different zooplankton taxa in the northern GSL (A,B) and the southwestern GSL (C, D) in June-July (A, C) and August-September (B, D) calculated for each stations. Only krill 500 m-bins overlapping with copepods stations were retained. The lower and upper hinges correspond to the 25th and 75th percentiles and the black horizontal bar to the median. The whiskers extend to the lower and upper value at most 1.5 * the inter-quartile range. Black circles are considered as outliers. The y-axis is represented on a logarithm scale (log10(x+1)). See figures 6 and 7 for spatial distribution of the depth integrated energy.*

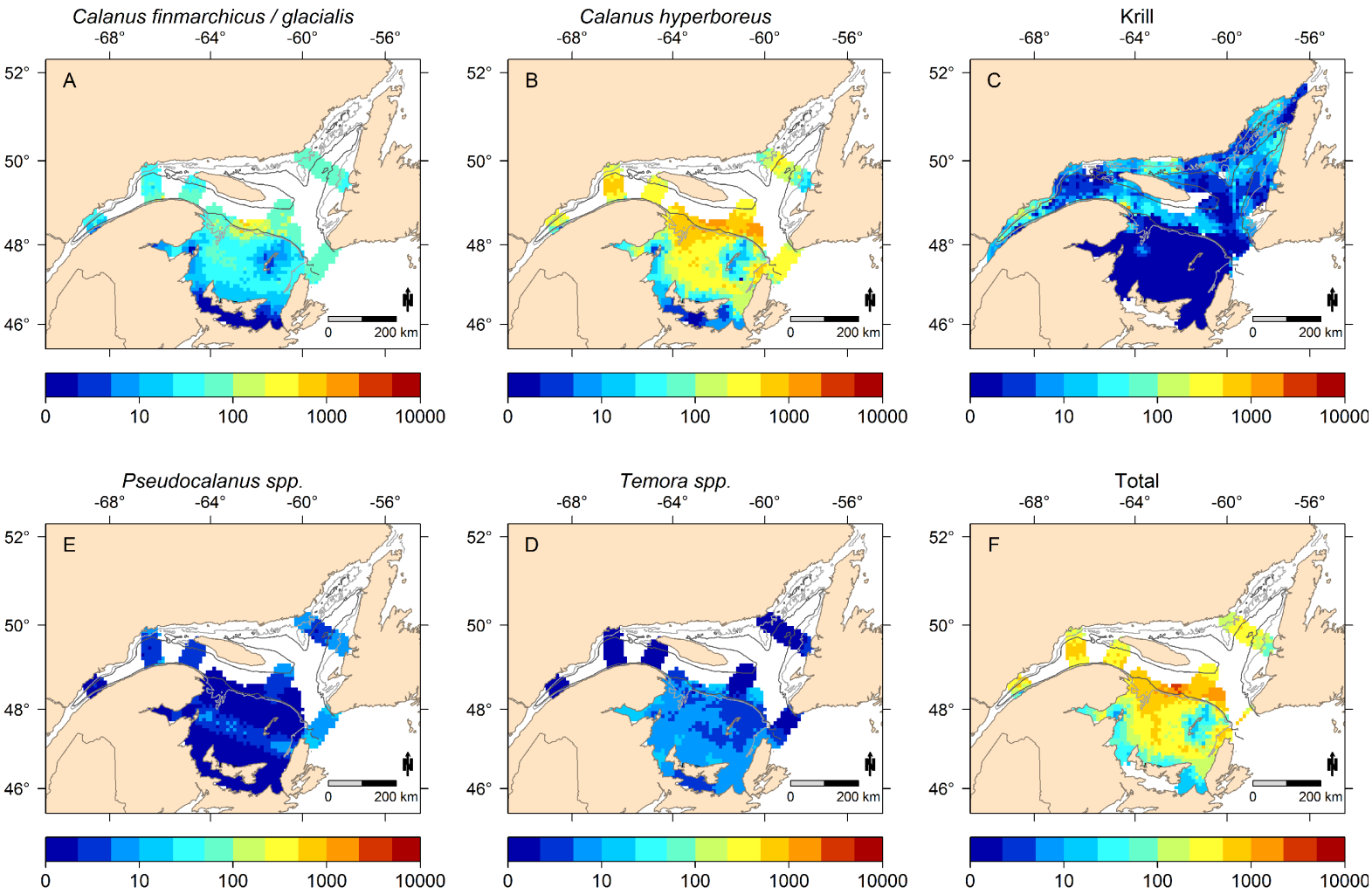


*Figure 8. Depth integrated energy (kJ $m^{-2}$) in June-July 2006-2017 for the different zooplankton taxa (A-D) and all taxa combined (F). The colorscale is represented on a logarithm scale.*

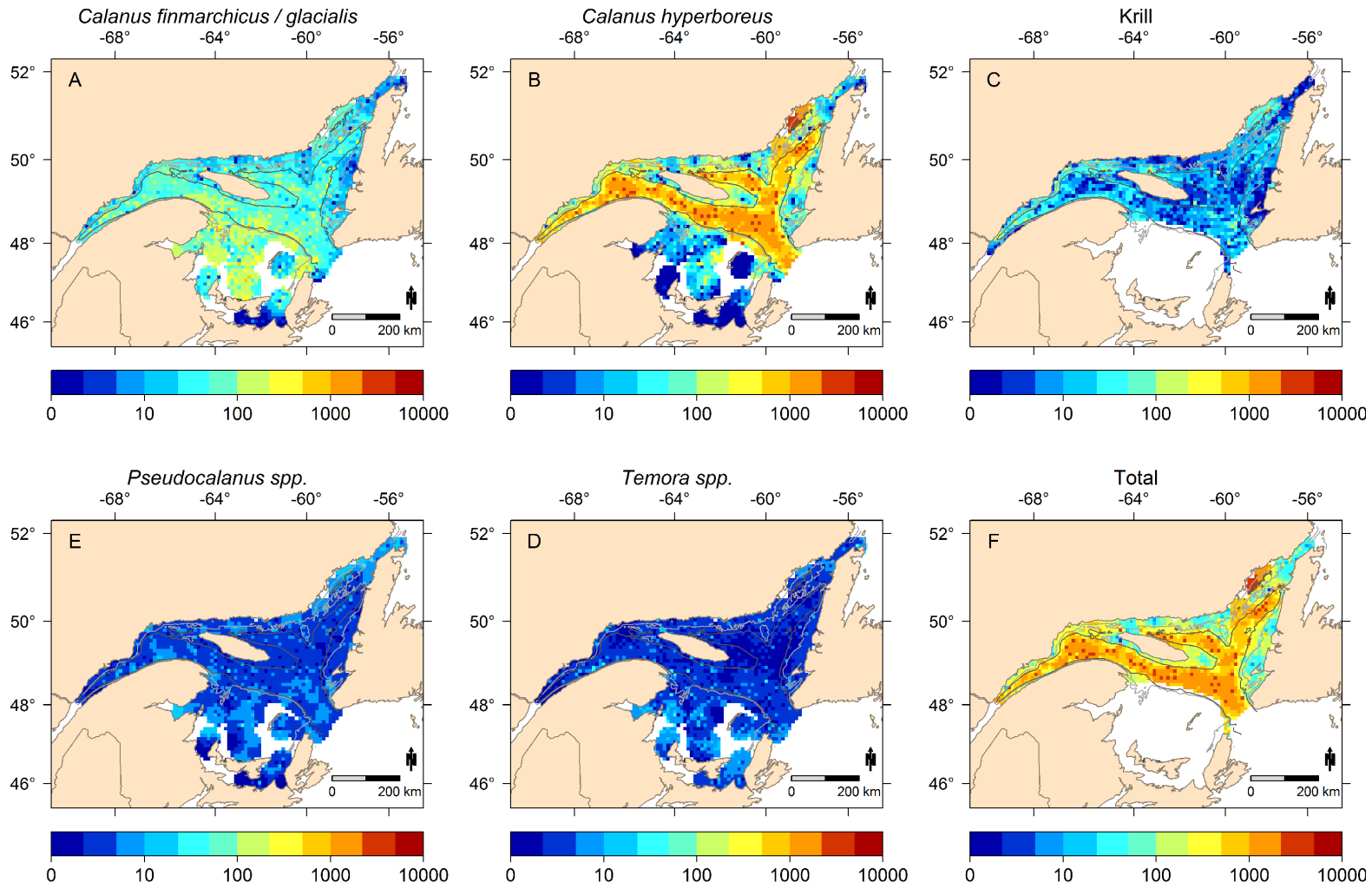


*Figure 9. Depth integrated energy (kJ m$^{-2}$) in August-September 2006-2017 for each prey (A-D) and all taxa combined (F). The colorscale is represented on a logarithm scale.*

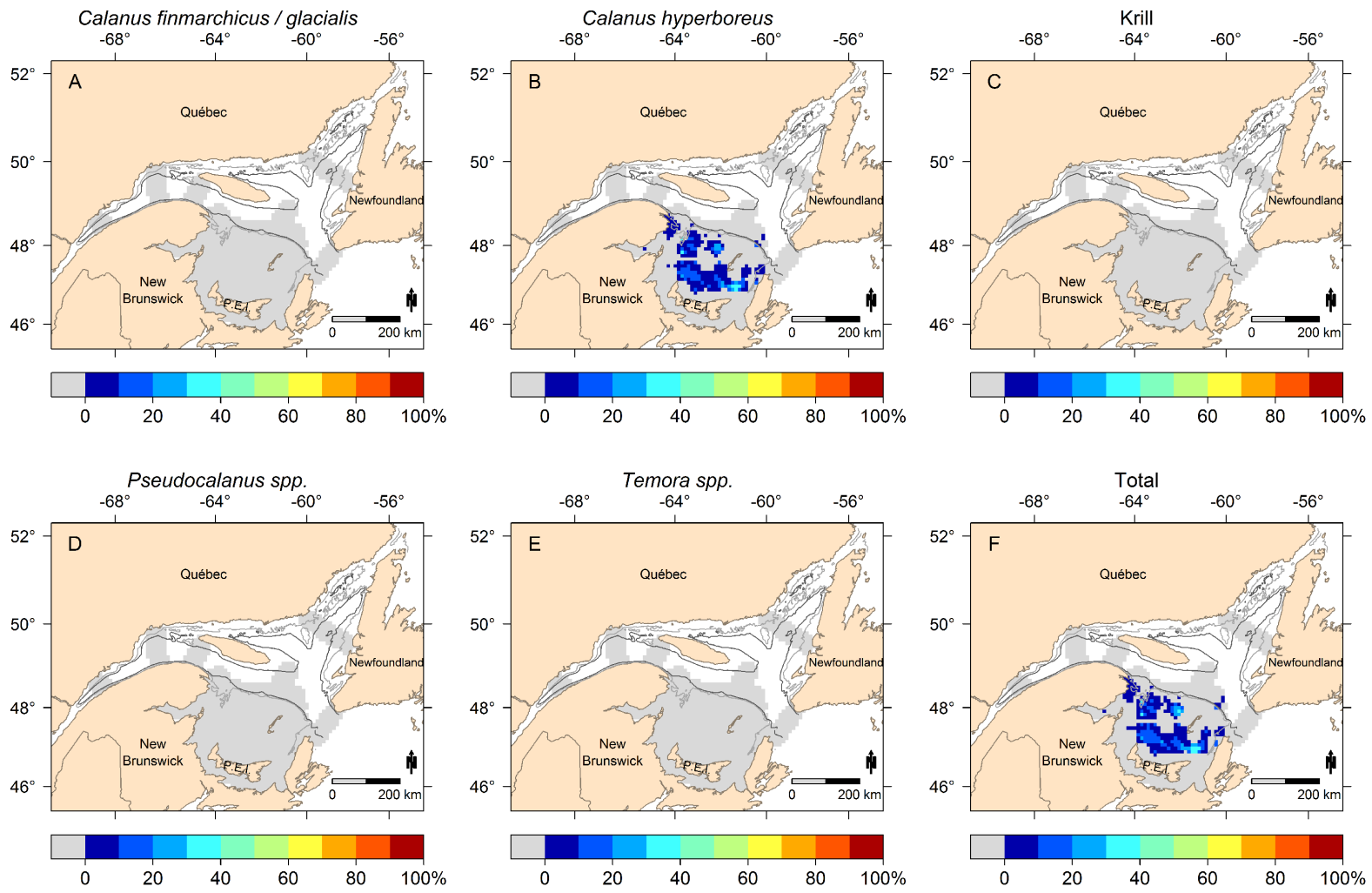


*Figure 10. Predicted suitable foraging habitat (percentage of years with $E_{net}$ >0) in June-July 2006-2017 for the different zooplankton taxa (A-E) and for all species added to the preyscape (F). The scale bar indicate the percentage of years where the energy requirement of pregnant whale is met (Enet >=0) while considering the mean of each parameter. Areas in grey were sampled but the $E_{net}$ is negative for all years.*

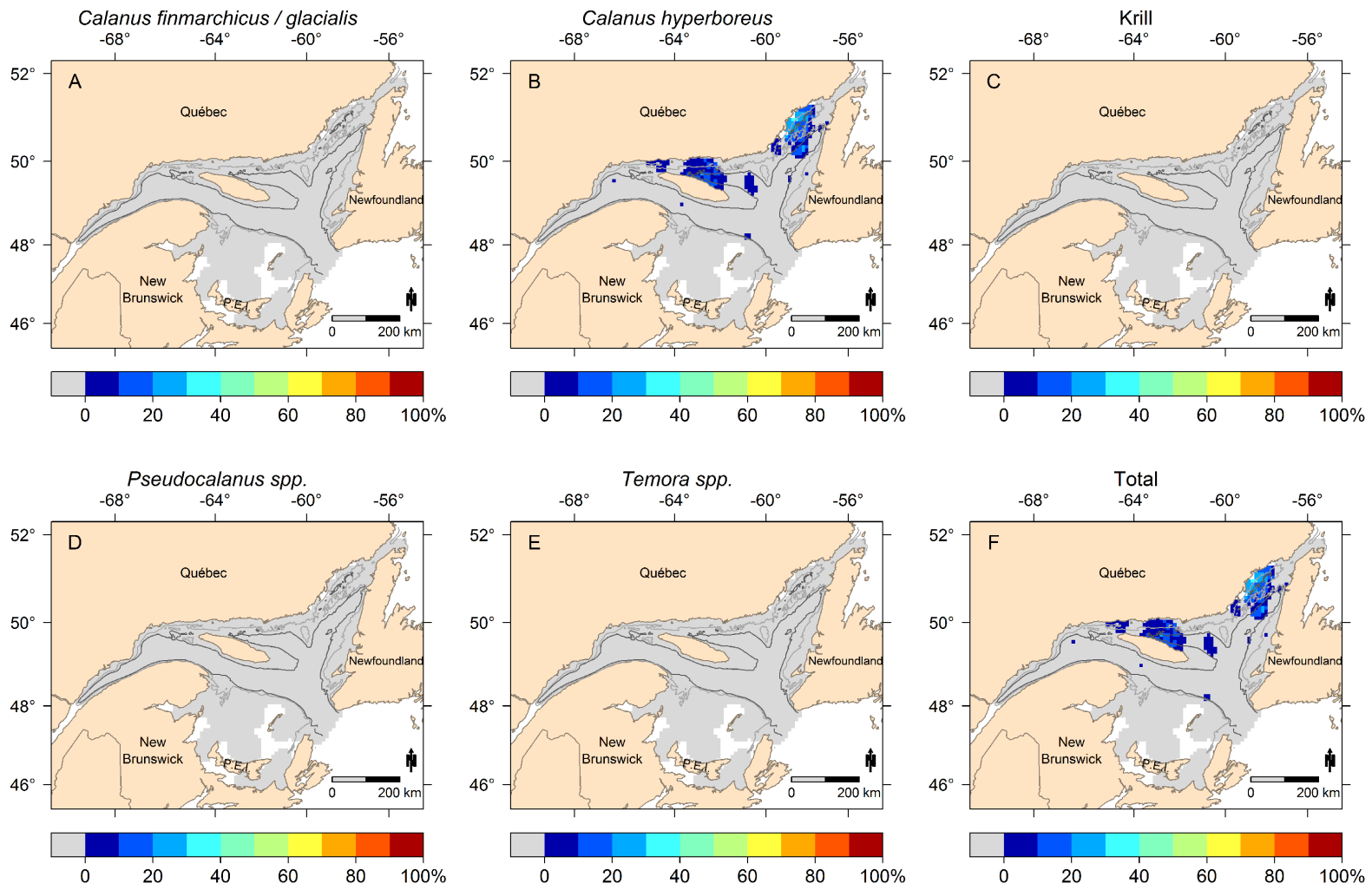


*Figure 11. Predicted suitable foraging habitat (percentage of years with $E_{net}$ >0) in August-September 2006-2017 for the different zooplankton taxa (A-E) and for all species added to the preyscape (F). The scale bar indicates the percentage of years where the energy requirement of pregnant whale is met ($E_{net}$ >=0) while considering the mean of each parameter. Areas in grey were sampled but the $E_{net}$ is negative for all years. The total in the SWGSL (F) corresponds to copepods but it includes krill in the NGSL.*

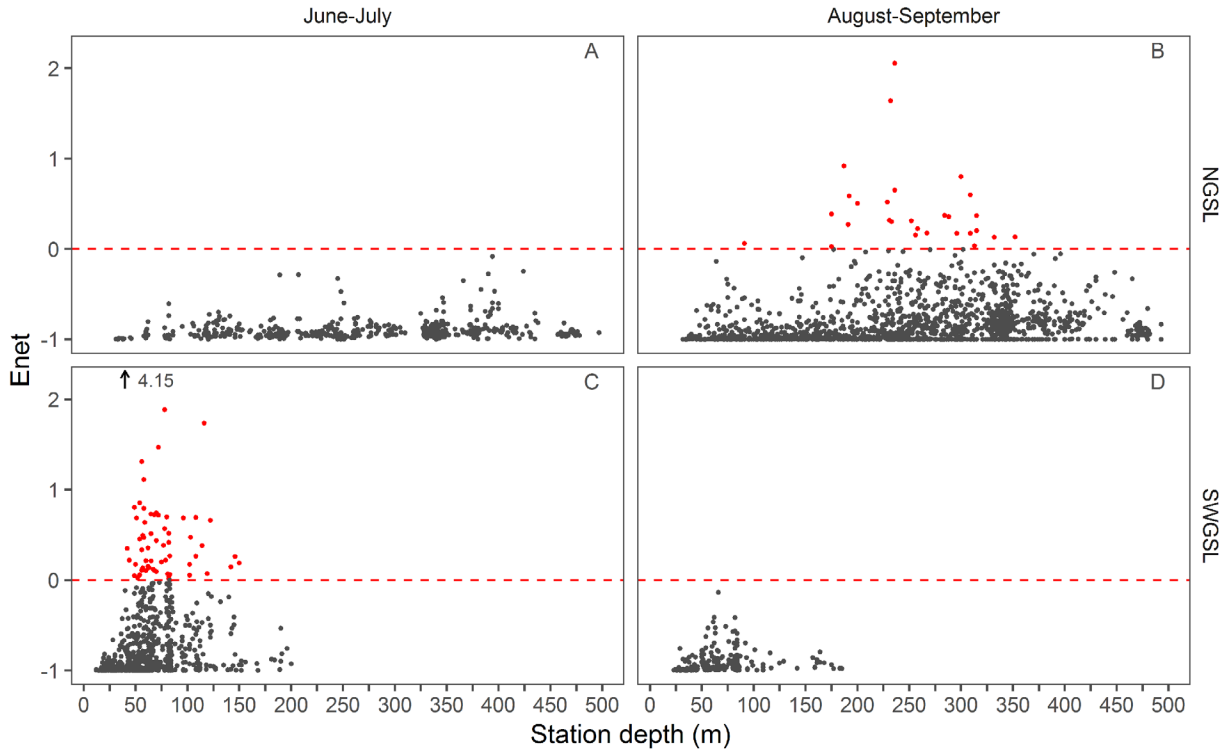


*Figure 12. Maximum $E_{net}$ for all stations sampled according to station depth in the NGSL (A, C) and the SWGSL (B, D) in June-July (A, B) and August-September (C, D) when considering the copepods as preys. Stations were sampled between 2006 and 2017. Red points above the red dashed line are suitable for pregnant females considering the mean of each parameter.*

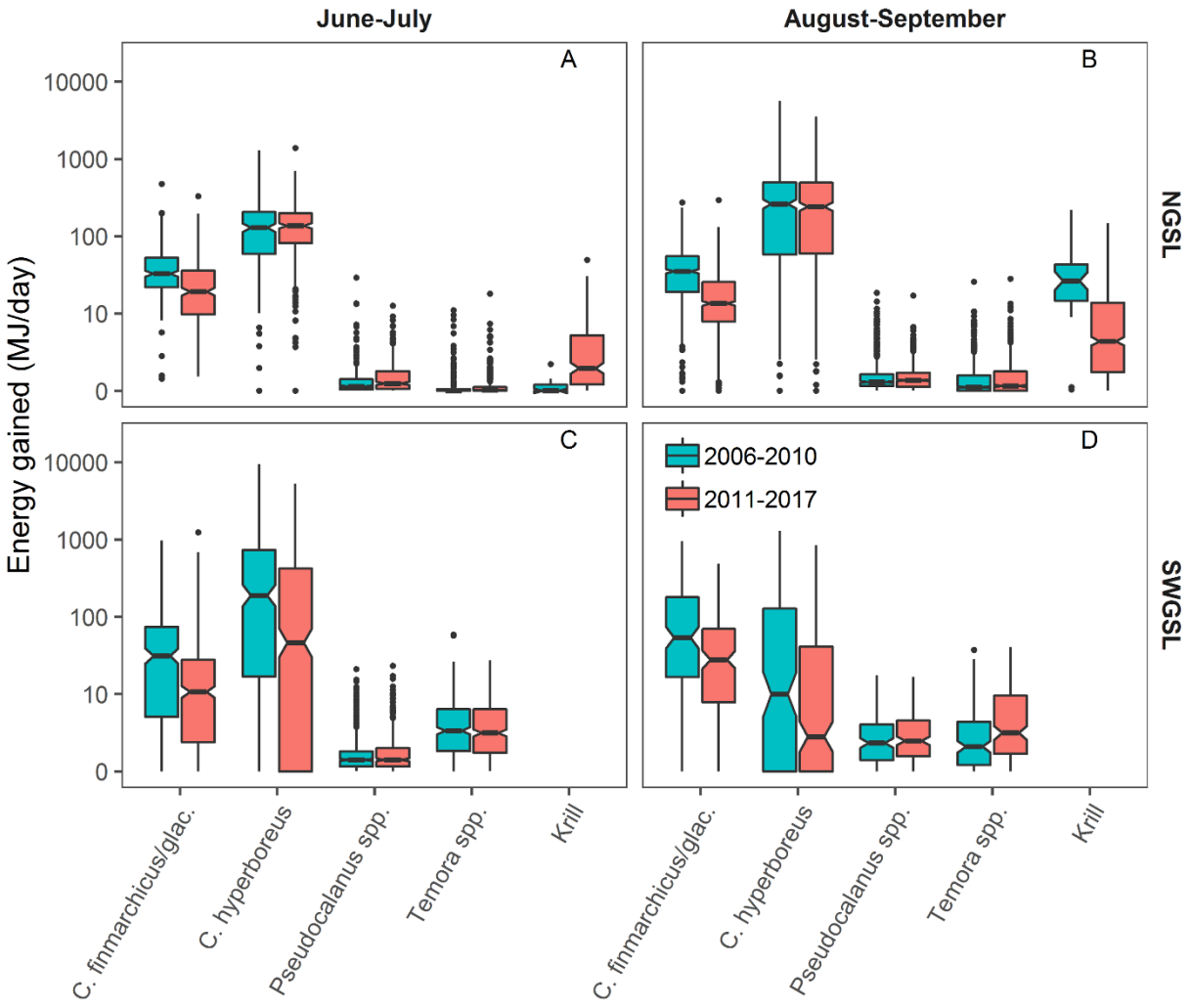


*Figure 13. Energy gained ($E_{in}$, MJ day$^{-1}$) in June-July (A,C) and August-September (C,D) in the NGSL (A,B) and the SWGSL (C,D) for the stations sampled in 2006-2010 (blue) and in 2011-2017 period (orange).The lower and upper hinges correspond to the 25th and 75th percentiles and the black horizontal bar to the median. The whiskers extend to the lower and upper value at most 1.5 * the inter-quartile range. Circles are considered as outliers. The y-axis is represented on a logarithm scale (log10(x+1)). Notches of boxplot that do not overlap suggest significant differences.*

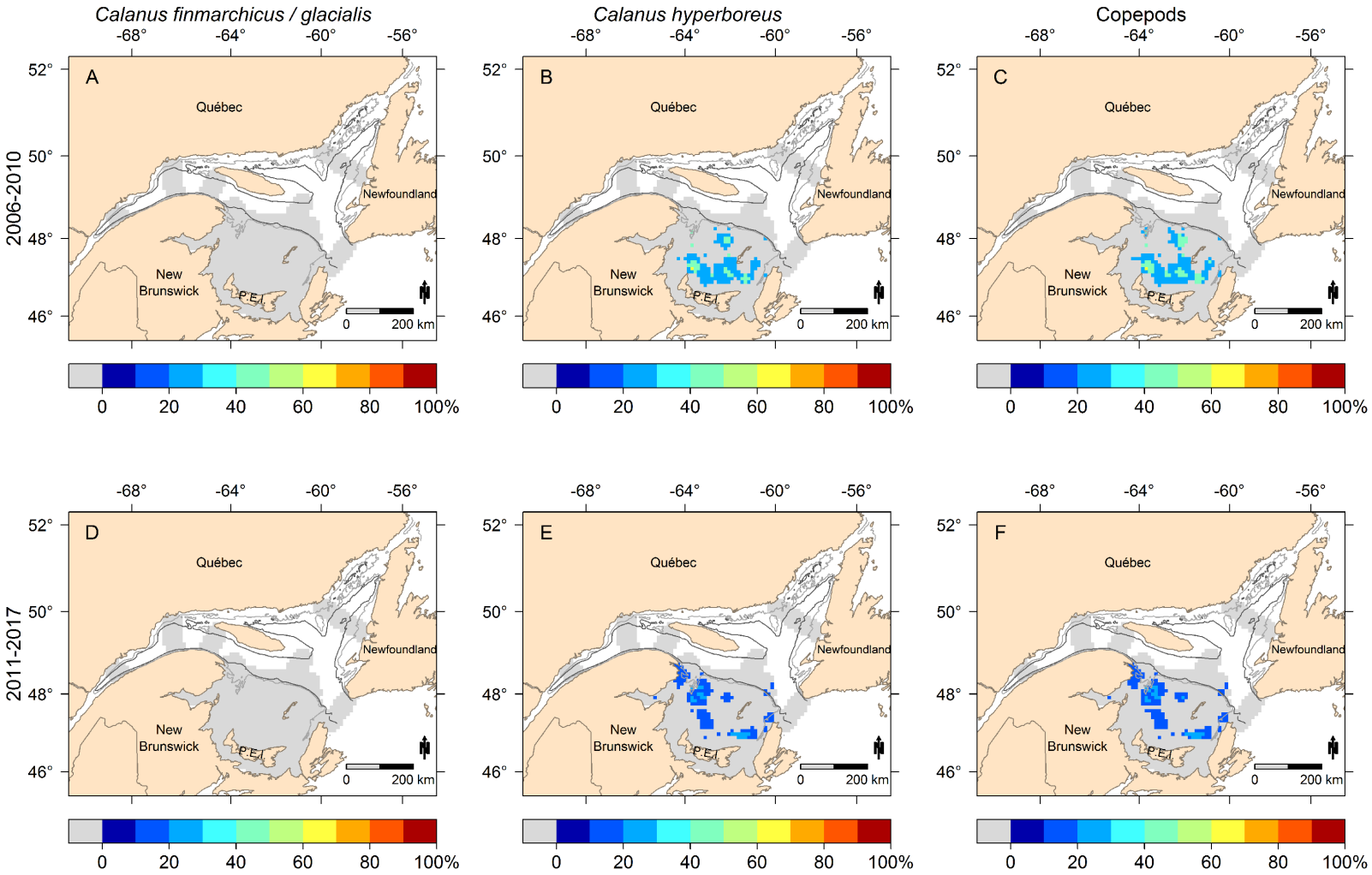


*Figure 14. Predicted suitable foraging habitat (percentage of years with $E_{net}$ >0) in June-July for Calanus finmarchicus/ glacialis (A,D), Calanus hyperboreus (B, E) and all four copepods taxa combined (C,F) during the 2006-2010 period (A-C) and the 2011-2017 period (D-F). The scale bar indicates the percentage of years where the energy requirement of pregnant whale is met ($E_{net}$ >=0) while considering the mean of each parameter. Areas in grey were sampled but the $E_{net}$ is negative for all years.*

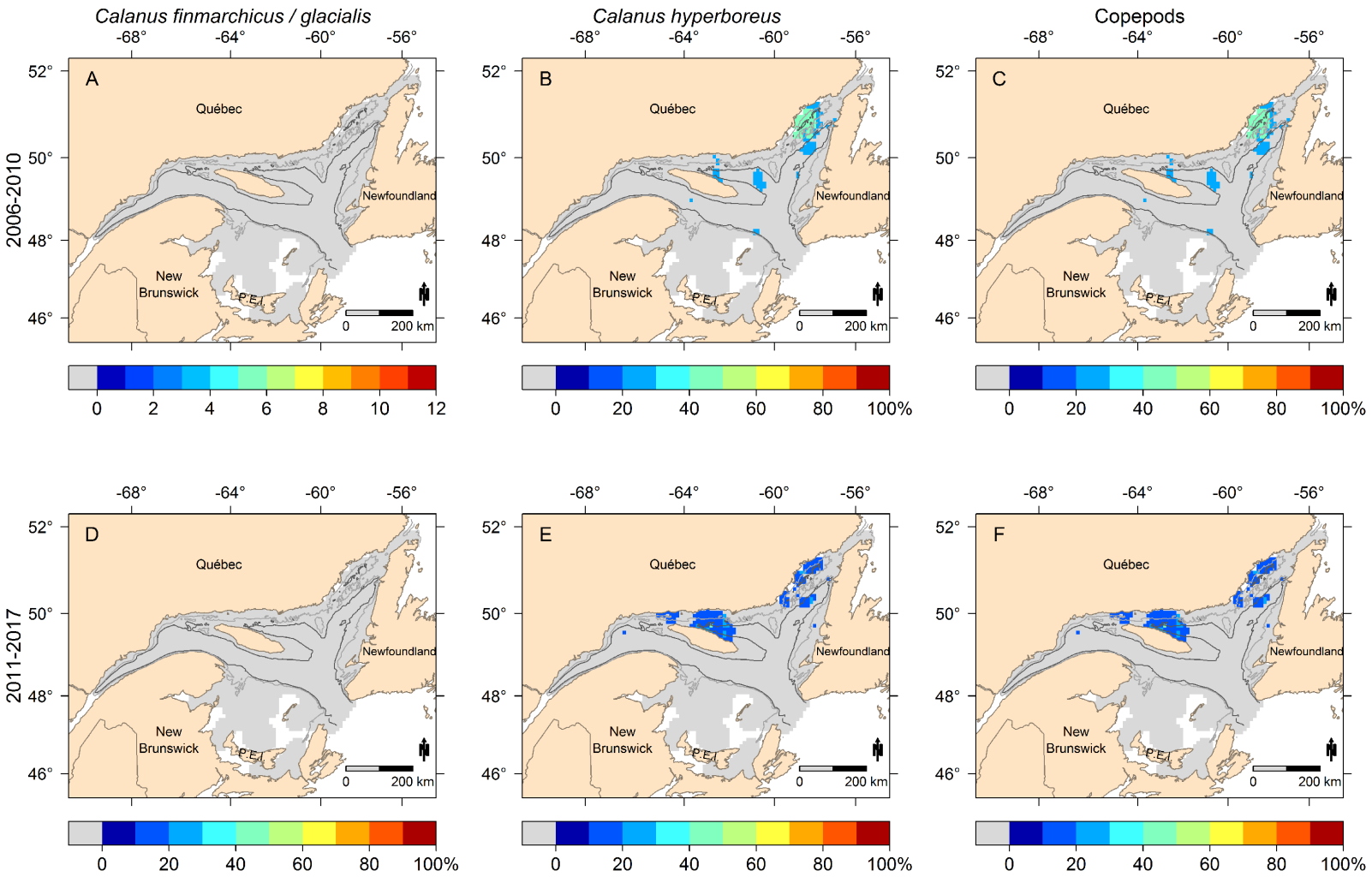


*Figure 15. Predicted suitable foraging habitat (percentage of years with $E_{net}$ >0) in August-September for Calanus finmarchicus/ glacialis (A,D), Calanus hyperboreus (B, E) and all four copepods taxa combined (C,F) during the 2006-2010 period (A-C) and the 2011-2017 period (D-F). The scale bar indicates the percentage of years where the energy requirement of pregnant whale is met ($E_{net}$ >=0) while considering the mean of each parameter. Areas in grey were sampled but the $E_{net}$ is negative for all years.*

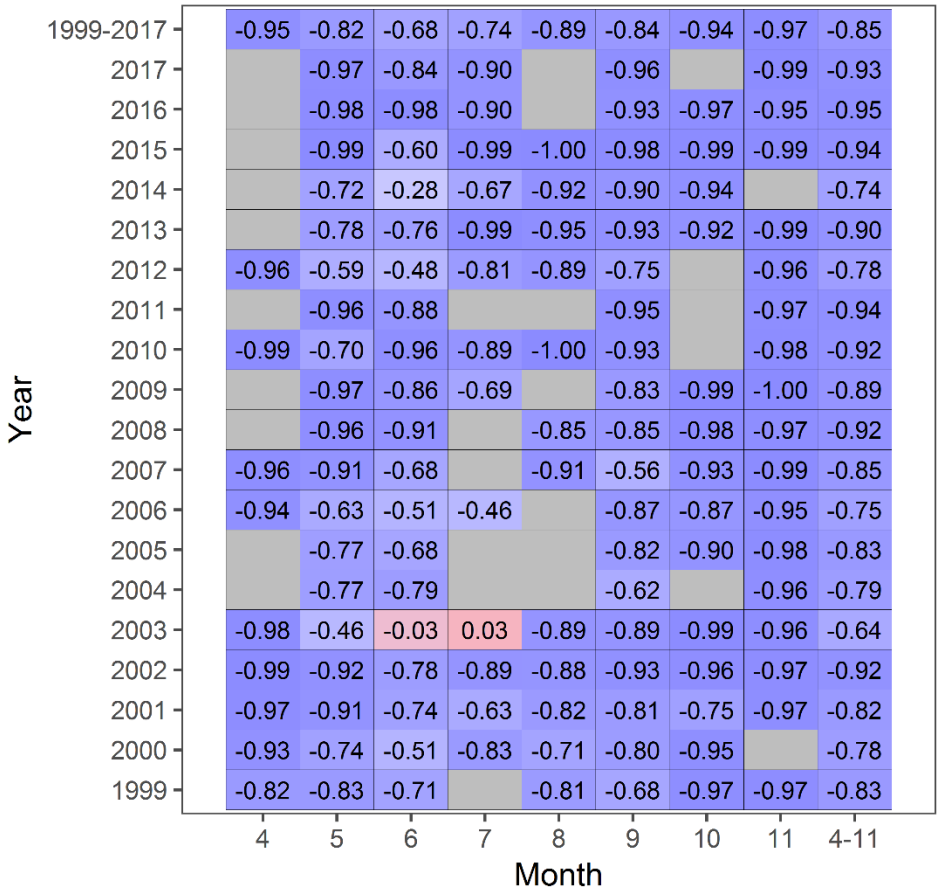


*Figure 16. Net energy index ($E_{net}$) at Shediac fixed station between April and November 1999 to 2017 and the annual mean (far right) and monthly mean (top). The net energy index is calculated by selecting the maximum $E_{net}$ for each sampling event which are then averaged in each tile.*

# APPENDIX 1

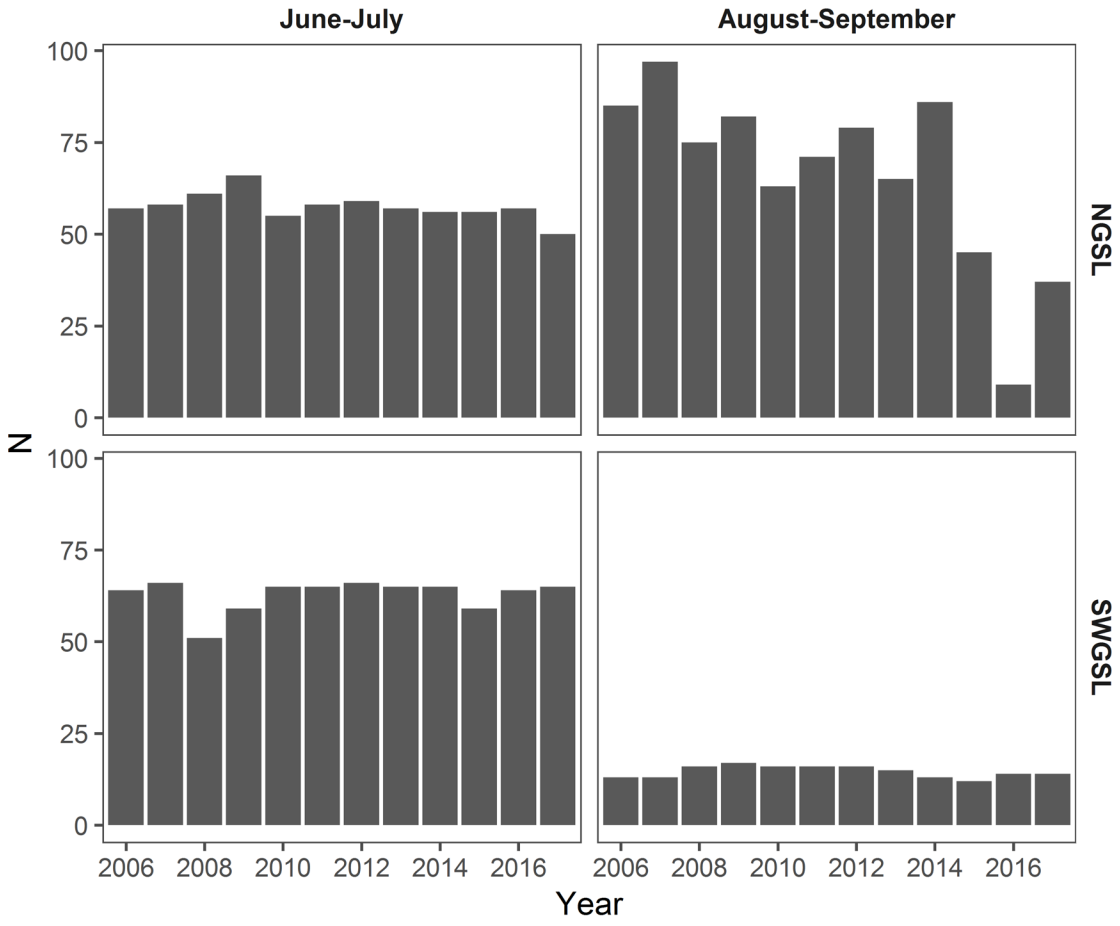


*Figure A.1.1. Number of stations (N) where copepods were sampled during June-July (left) and August-September (right) in the Lower St Lawrence Estuary (SLE) and Northern Gulf (NGSL) and South-Western Gulf of St Lawrence (SWGSL) between 2006 and 2017.*

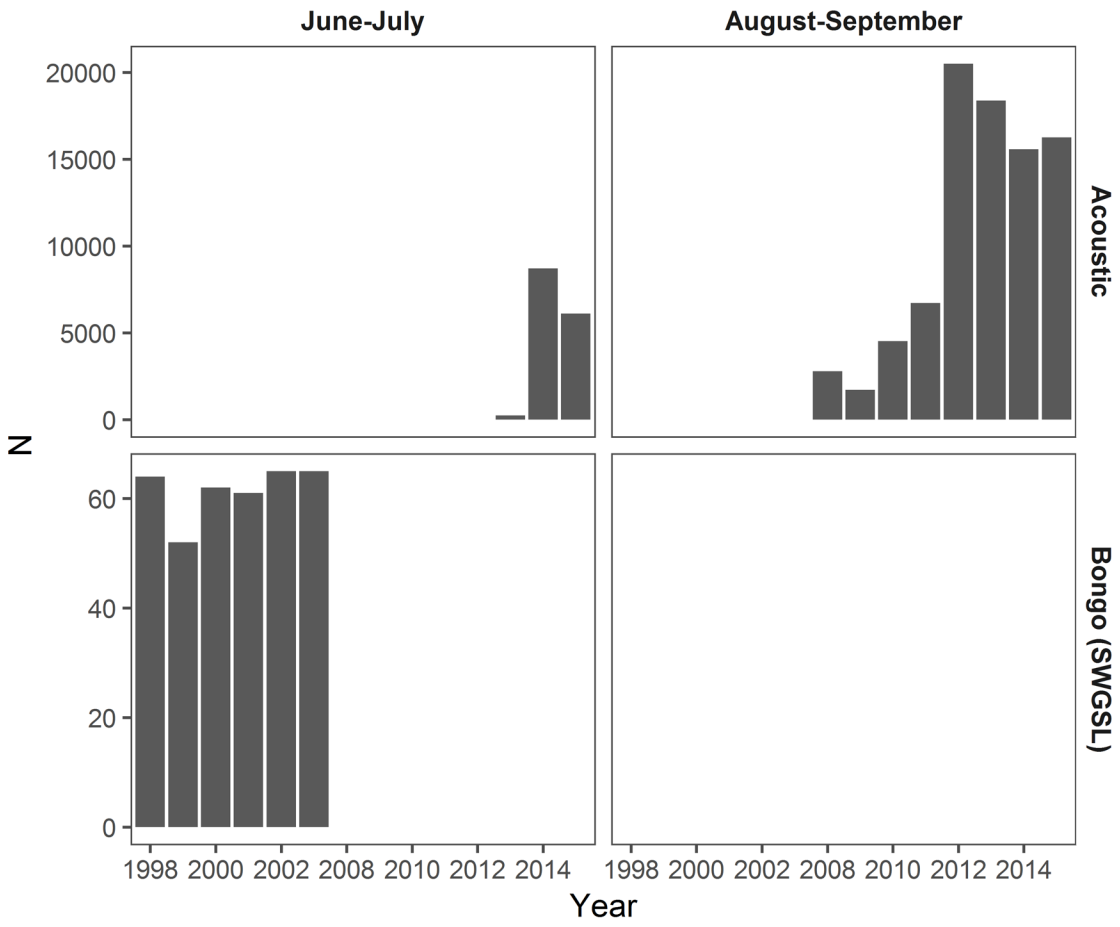


*Figure A.1.2. Number of stations (N) or 500m-bins (for acoustic data) included for krill in the bioenergetics model in June-July (left) and August-September (right) using multifrequency acoustics (NGSL) or Bongo (SWGSL) between 1998 and 2015.*

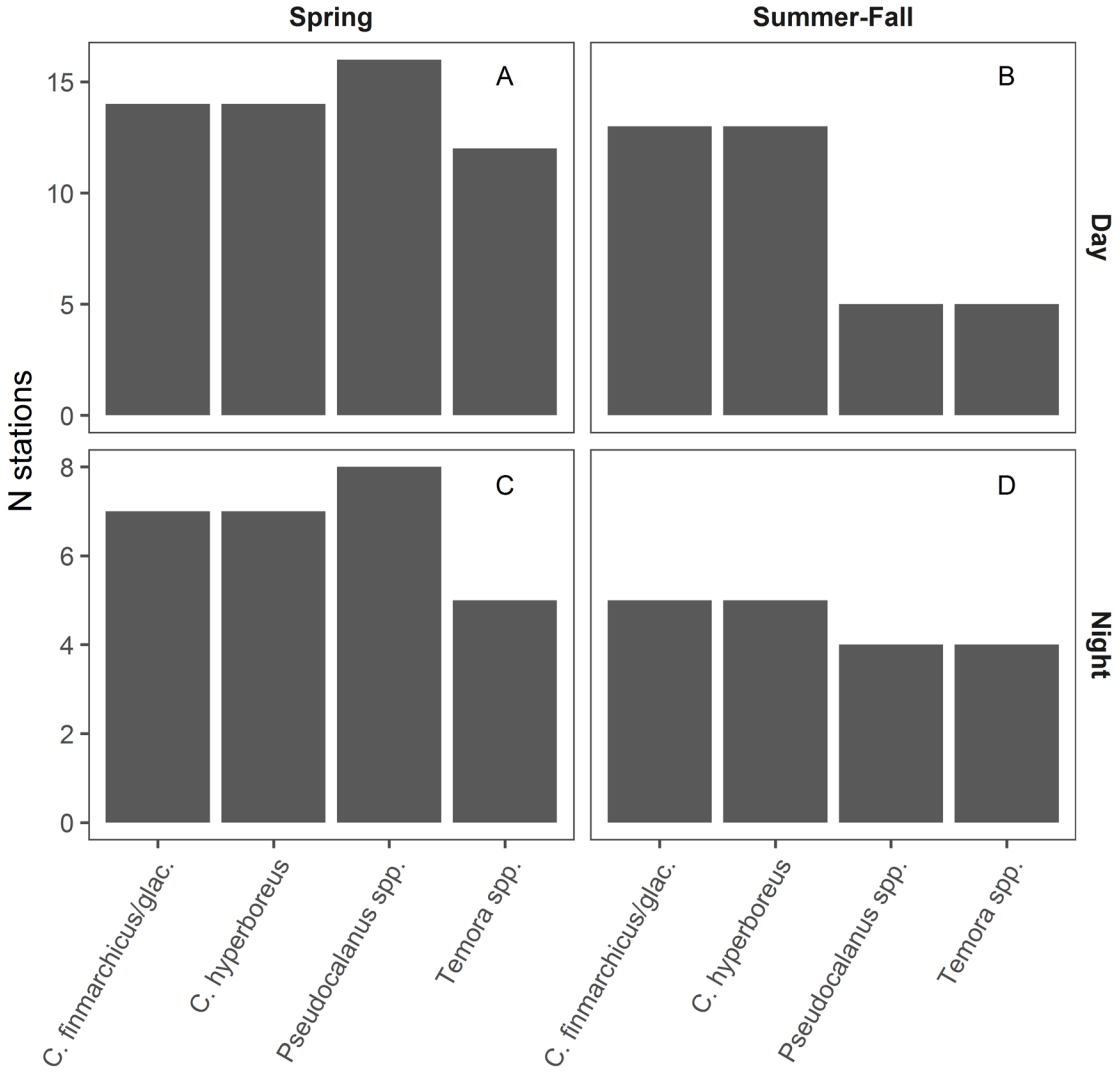


*Figure A.1.3. Number of stations (N) used in GAMs for each copepod species for Spring (A, C) and Summer-Fall (B,D) during the day (A, B) and night (C, D). For Calanus spp. GAMs, data were restricted to June, August and September. Pseudocalanus spp. and Temora spp. were sampled during June and November. Temora spp. was not systematically identified by taxonomists each year which is why it has a lower N than Pseudocalanus spp.*

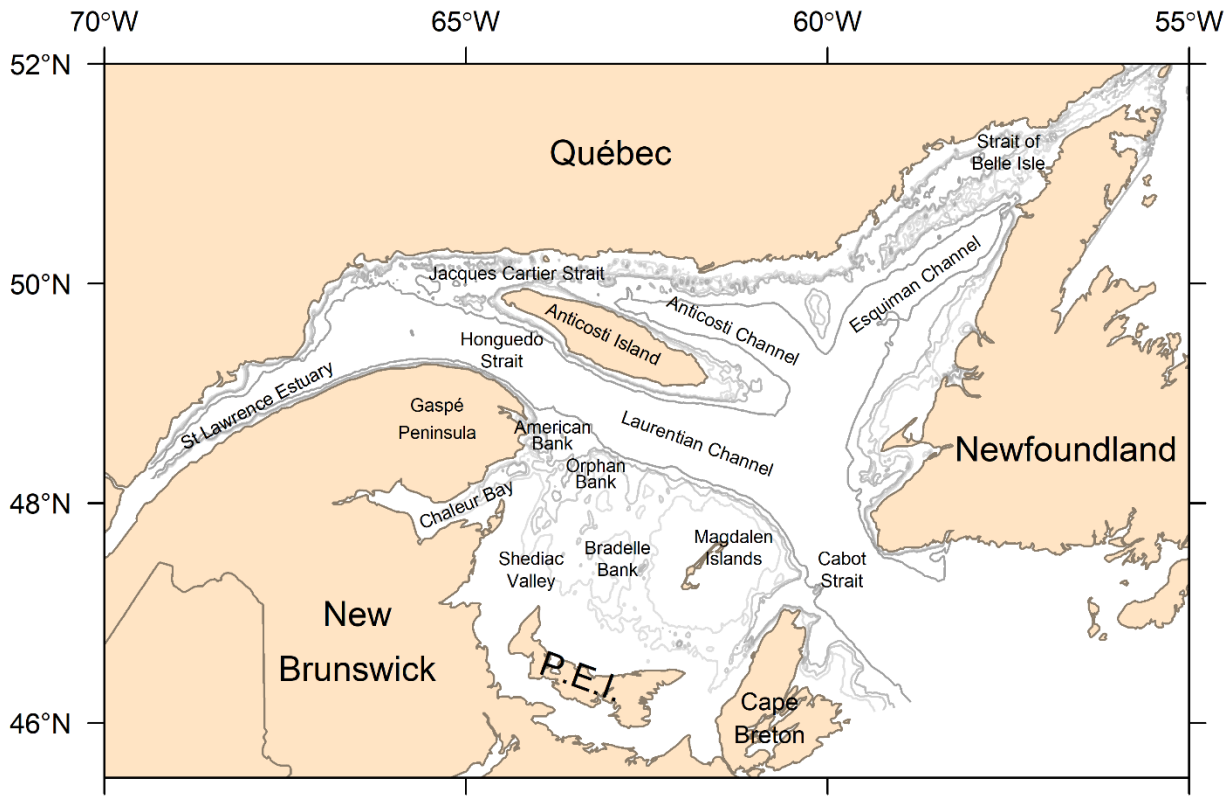


*Figure A.1.4. Study area with important geographic and topographic features. Dark to light grey lines: 200 m, 100 m, 80 m, and 60 m isobaths.*

# APPENDIX 2

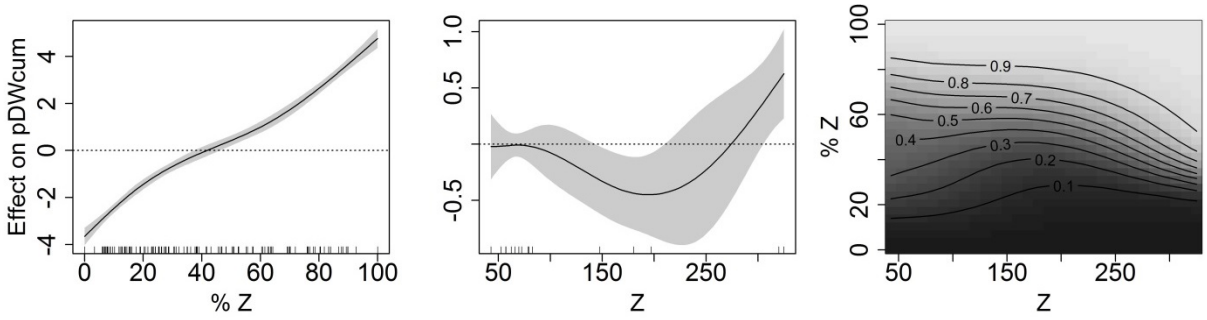


*Figure A.2.1. Results of GAMs showing the effect of the percentage of the depth sampled (%Z), the depth of the station (Z) and the interaction between the %Z and the Z on the proportion of the total biomass (pDWcum) of Calanus finmarchicus /glacialis sampled during the day in the GSL in June (see results Table 2). The 95 % confidence intervals (shaded areas) included the error on the overall mean. The horizontal dashed line 0 represent the intercept with positive and negative effect of the %Z and the Z above and under the line respectively. The effect of the interaction between the %Z and the Z on the pDWcum is represented by the contour lines. Numbers on the contour lines represent the pDWcum, lighter shades of grey represent a more positive effect on the pDWcum.*

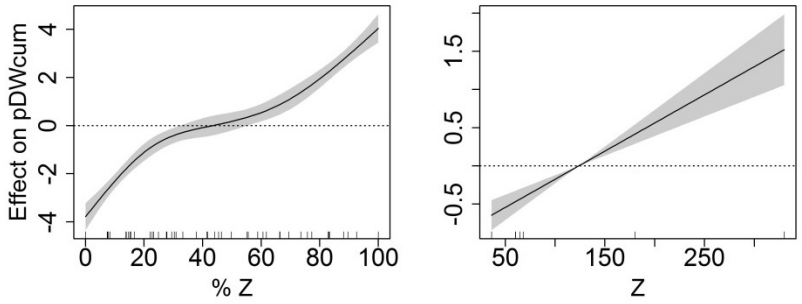


*Figure A.2.2. Results of GAMs showing the effect of the percentage of the depth sampled (%Z) and the depth of the station (Z) on the proportion of the total biomass (pDWcum) of Calanus finmarchicus /glacialis sampled during the night in the GSL in June (see Table 2 and Figure A.2.1 for details).*

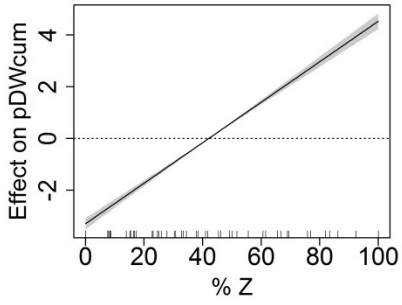


*Figure A.2.3. Results of GAMs showing the effect of the percentage of the depth sampled (%Z) on the proportion of the total biomass (pDWcum) of Calanus finmarchicus /glacialis sampled during the day in the GSL in August-September (see Table 2 and Figure A.2.1 for details).*

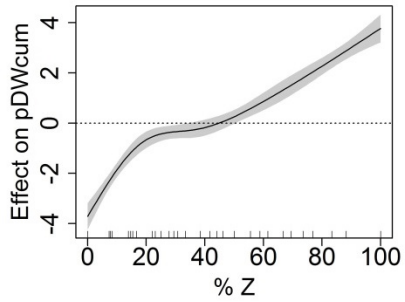


*Figure A.2.4. Results of GAMs showing the effect of the percentage of the depth sampled (%Z) on the proportion of the total biomass (pDWcum) of Calanus finmarchicus /glacialis sampled during the night in the GSL in August-September (see Table 2 and Figure A.2.1 for details).*

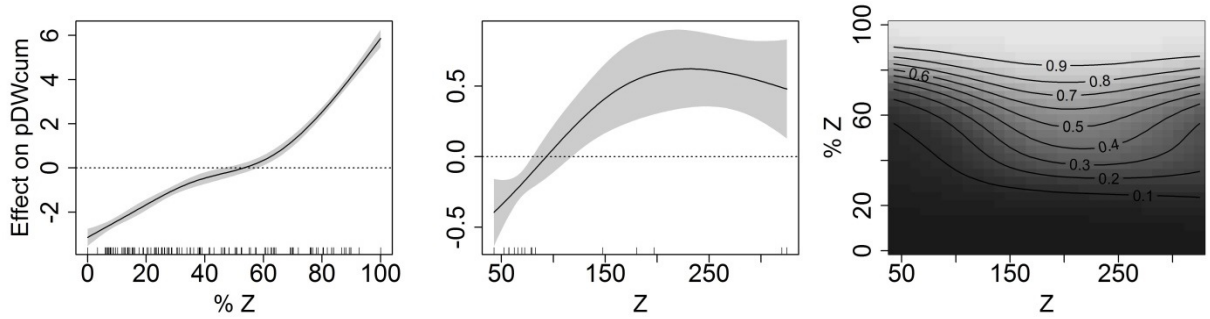


*Figure A.2.5. Results of GAMs showing the effect of the percentage of the depth sampled (%Z), the depth of the station (Z) and the interaction between the %Z and the Z on the proportion of the total biomass (pDWcum) of Calanus hyperboreus sampled during the day in the GSL in June (see Table 2 and Figure A.2.1 for details).*

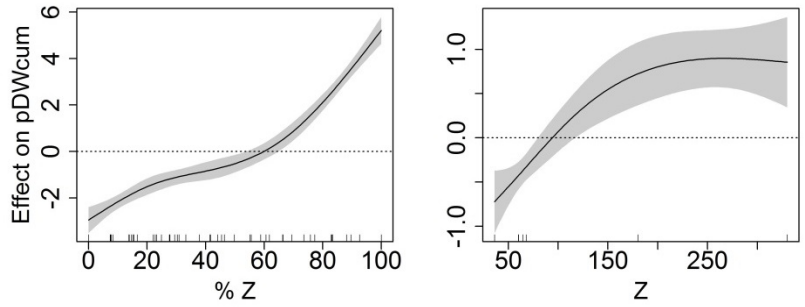


*Figure A.2.6. Results of GAMs showing the effect of the percentage of the depth sampled (%Z) and the depth of the station (Z) on the proportion of the total biomass (pDWcum) of Calanus hyperboreus sampled during the night in the GSL in June (see Table 2 and Figure A.2.1 for details).*

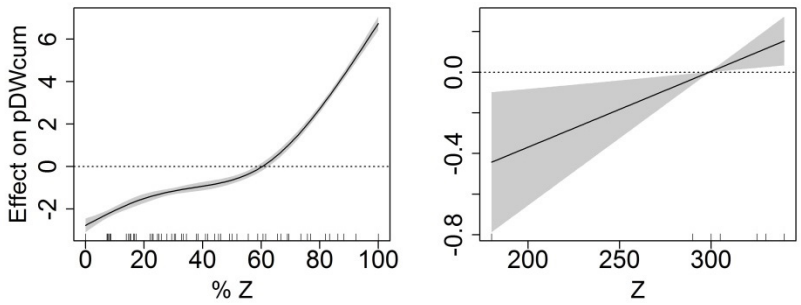


*Figure A.2.7. Results of GAMs showing the effect of the percentage of the depth sampled (%Z) and the depth of the station (Z) on the proportion of the total biomass (pDWcum) of Calanus hyperboreus in the GSL in August-September (see Table 2 and Figure A.2.1 for details).*

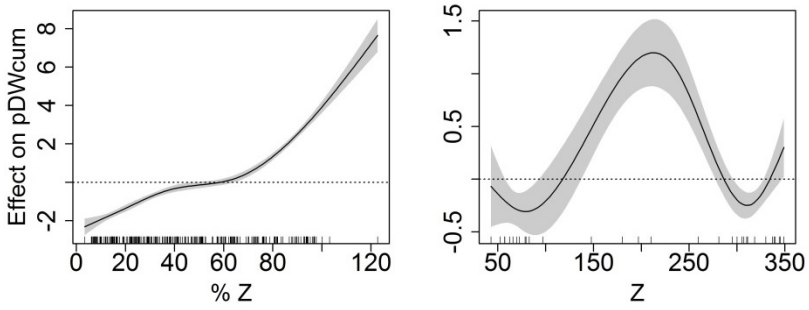


*Figure A.2.8. Results of GAMs showing the effect of the percentage of the depth sampled (%Z) and the depth of the station (Z) on the proportion of the total biomass (pDWcum) of Pseudocalanus sampled during the day in the GSL (see Table 2 and Figure A.2.1 for details).*

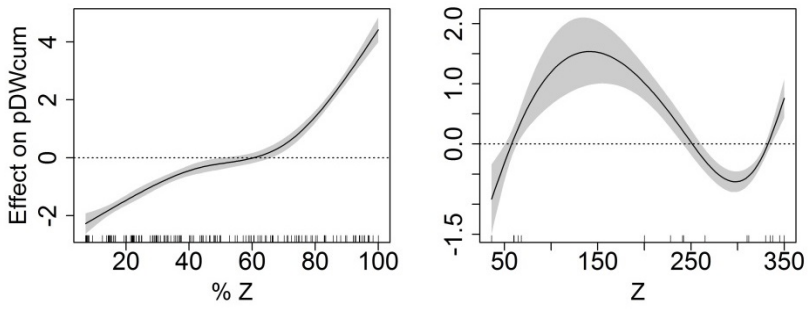


*Figure A.2.9. Results of GAMs showing the effect of the percentage of the depth sampled (%Z) and the depth of the station (Z) on the proportion of the total biomass (pDWcum) of Pseudocalanus sampled during the night in the GSL (see Table 2 and Figure A.2.1 for details).*

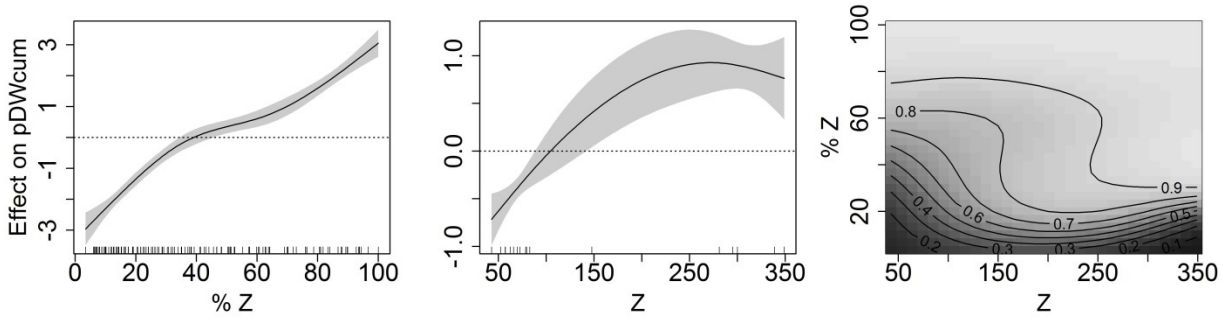


*Figure A.2.10. Results of GAMs showing the effect of the percentage of the depth sampled (%Z), the depth of the station (Z) and the interaction between the %Z and the Z on the proportion of the total biomass (pDWcum) of Temora spp. sampled during the day in the GSL (see Table 2 and Figure A.2.1 for details).*

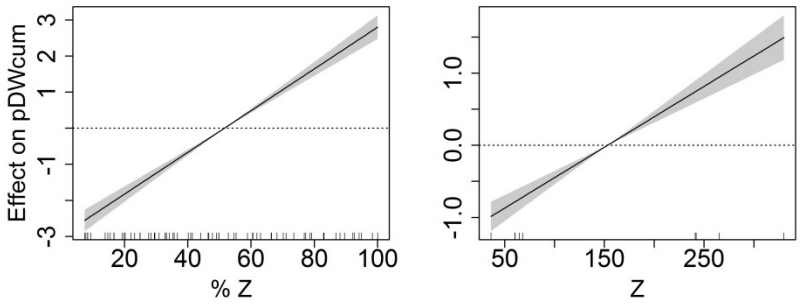


*Figure A.2.11. Results of GAMs showing the effect of the percentage of the depth sampled (%Z) and the depth of the station (Z) on the proportion of the total biomass (pDWcum) of Temora spp. sampled during the night in the GSL (see Table 2 and Figure A.2.1 for details).*

# APPENDIX 3

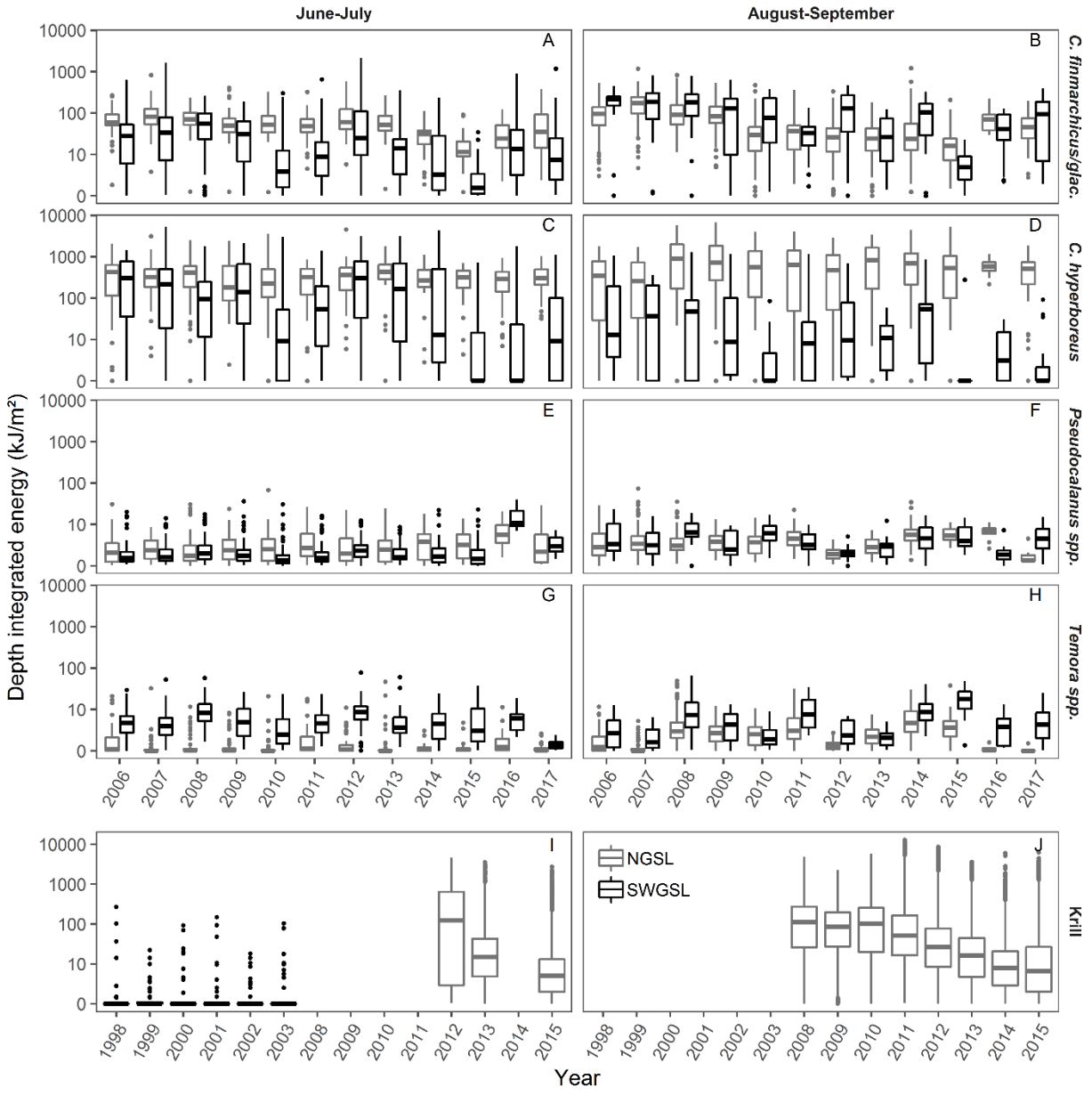


*Figure A.3.1. Depth integrated energy (kJ/m²) for each taxa at sampled stations for each year in the NGSL (grey) and SWGSL (black) in June-July (A, C,E,G,I) and August-September (B, D,F,H,J). The lower and upper hinges correspond to the 25th and 75th percentiles and the black horizontal bar to the median. The whiskers extend to the lower and upper value at most 1.5 * the inter-quartile range. Circles are considered as outliers. The y-axis is represented on a logarithm scale (log10(x+1)).*